AD-A214 595

A COMPARISON OF THE SPECTRAL CHARACTERISTICS OF NUCLEAR

EXPLOSIONS DETONATED BELOW AND ABOVE THE WATER TABLE

I. N. Gupta
C. S. Lynnes
W. W. Chan
R. A. Wagner

Teledyne Geotech Alexandria Laboratories
314 Montgomery Street
Alexandria, VA 22314-1581

April 1989

Scientific Report No. 1

GEOPHYSICS LABORATORY
AIR FORCE SYSTEMS COMMAND
UNITED STATES AIR FORCE
HANSCOM AIR FORCE BASE, MASSACHUSETTS 01731-5000

DTIC
ELECTE
NOV.24 1989
S B D

89 11 21 137

The views and conclusions contained in this document are those of the authors and should not be interpreted as representing the official policies, either expressed or implied, of the Defense Advanced Research Projects Agency or the U.S. Government.

This technical report has been reviewed and is approved for publication.

JAMES F. LEWKOWICZ
Contract Manager
Solid Earth Geophysics Branch
Earth Sciences Division

JAMES F. LEWKOWICZ
Branch Chief
Solid Earth Geophysics Branch
Earth Sciences Division

FOR THE COMMANDER
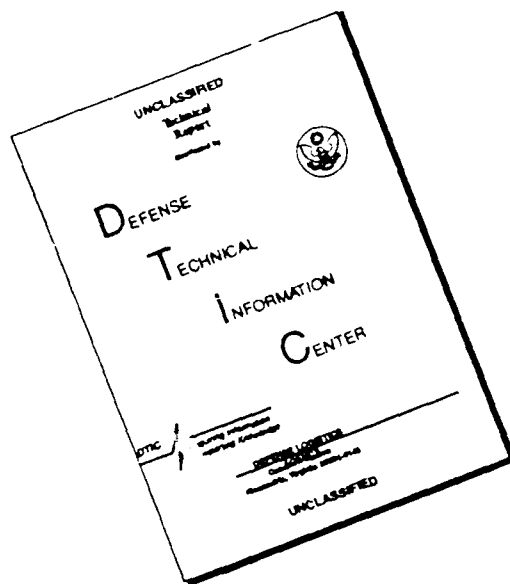
DONALD H. ECKHARDT, Director
Earth Sciences Division

DISCLAIMER NOTICE

THIS DOCUMENT IS BEST QUALITY AVAILABLE. THE COPY FURNISHED TO DTIC CONTAINED A SIGNIFICANT NUMBER OF PAGES WHICH DO NOT REPRODUCE LEGIBLY.

REPORT DOCUMENTATION PAGE

Form Approved
OMB No 0704 0188
Exp Date Jun 30 1986

1a REPORT SECURITY CLASSIFICATION	1b RESTRICTIVE MARKINGS
Unclassified	

2a SECURITY CLASSIFICATION AUTHORITY	3 DISTRIBUTION/AVAILABILITY OF REPORT
	Approved for public release;
2b DECLASSIFICATION/DOWNGRADING SCHEDULE	Distribution unlimited.

4 PERFORMING ORGANIZATION REPORT NUMBER(S)	5 MONITORING ORGANIZATION REPORT NUMBER(S)
TGAL-89-04	GL-TR-89-0151

6a NAME OF PERFORMING ORGANIZATION	6b OFFICE SYMBOL (If applicable)	7a NAME OF MONITORING ORGANIZATION
Teledyne Geotech	TGAL	Geophysics Laboratory

6c ADDRESS (City, State, and ZIP Code)	7b ADDRESS (City, State, and ZIP Code)
314 Montgomery Street Alexandria, VA 22314	Hanscom AFB, MA 01731-5000

8a NAME OF FUNDING/SPONSORING ORGANIZATION	8b OFFICE SYMBOL (If applicable)	9 PROCUREMENT INSTRUMENT IDENTIFICATION NUMBER
DARPA	NMRO	F19628-88-C-0051

8c ADDRESS (City, State, and ZIP Code)	10 SOURCE OF FUNDING NUMBERS			
1400 Wilson Blvd. Arlington, VA 22209-2308	PROGRAM ELEMENT NO	PROJECT NO	TASK NO	WORK UNIT ACCESSION NO
	62714E	8A10	DA	AA

11 TITLE (Include Security Classification)

A Comparison of the Spectral Characteristics of Nuclear Explosions Detonated Below and Above the Water Table

12 PERSONAL AUTHOR(S)

I.N. Gupta, C.S. Lynnes, W.W. Chan, R.A. Wagner

13a TYPE OF REPORT	13b TIME COVERED	14 DATE OF REPORT (Year, Month, Day)	15 PAGE COUNT
Scientific Report No.1	FROM Mar 88 TO Feb 89	April 89	78

16 SUPPLEMENTARY NOTATION

17 COSATI CODES			18 SUBJECT TERMS (Continue on reverse if necessary and identify by block number)
FIELD	GROUP	SUB GROUP	Spectral Characteristics, Water Table, Regional Phases, Pn, Lg, Gas Porosity

19 ABSTRACT (Continue on reverse if necessary and identify by block number)

A comparison of the spectra of nuclear shots detonated below and above the water table (WT) is made by analysis of mostly the regional phases Pn recorded at two common stations. Parameters derived from each record include estimates of corner frequency f_c and the low-frequency spectral level A_0, after the spectra have been corrected for the effects of spatial attenuation. The time-domain measurements of A/T, a measure of m_b, are also made on each observed record. Results from 22 Nevada Test Site (NTS) shots recorded at the DWWSSN digital station, JAS, indicate that plots of f_c versus A_0 show some separation between the below and above WT populations whereas plots of f_c versus A/T show no significant separation. For a fixed yield, f_c for shots below and above WT are nearly indistinguishable whereas both A_0 and A/T are considerably larger for shots below WT than for those above WT, presumably due to improved source coupling of shots in water saturated environment. A comparison of yields estimated from A_0, A/T, A_0 combined with f_c, and A/T combined with f_c demonstrates that substantially more precise yield determinations can be made if it is known whether the shot was

20 DISTRIBUTION/AVAILABILITY OF ABSTRACT	21 ABSTRACT SECURITY CLASSIFICATION
[ ] UNCLASSIFIED/UNLIMITED [ ] SAME AS RPT [ ] DTIC USERS	Unclassified

22a NAME OF RESPONSIBLE INDIVIDUAL	22b TELEPHONE (Include Area Code)	22c OFFICE SYMBOL
James Lewkowicz	(617) 377-3028	GL/LWH

DD FORM 1473, 84 MAR

83 APR edition may be used until exhausted
All other editions are obsolete

SECURITY CLASSIFICATION OF THIS PAGE

(19. continued)

detonated above or below WT. Results from the analysis of 17 NTS shots recorded at the RSTN station, RSSD are generally not as well defined but appear similar to those from the JAS recordings. The largest difference between the below and above WT shots of a given yield lies in their low-frequency spectral level and, to a slightly smaller extent, in their m_b values.

Examination of m_b versus yield from large data bases of NTS shots recorded at regional and teleseismic distances also shows that, for a fixed yield, shots below WT have significantly larger m_b than those detonated above WT. Gas-filled porosity of the shot medium appears to be the dominant reason for the large magnitude bias between below and above WT shots. For shots detonated near the water table, explosion cavity and its proximity to WT can also significantly influence the source coupling. Below and above WT shots may be distinguished by comparing their Pn and Lg phases at common recording stations.

Accession For

NTIS GRA&I	☑
DTIC TAB	☐
Unannounced	☐
Justification	

By
Distribution/
Availability Codes

Dist	Avail and/or Special
A-1	

SUMMARY

A comparison of the spectra of nuclear shots detonated below and above the water table (WT) is made by analysis of mostly the regional phase Pn recorded at two common stations. Parameters derived from each record include estimates of corner frequency f_c and the low-frequency spectral level A_0, after the spectra have been corrected for the effects of spatial attenuation. The time-domain measurements of A/T, a measure of m_b, are also made on each observed record. Results from 22 Nevada Test Site (NTS) shots recorded at the DWWSSN digital station, JAS, indicate that plots of f_c versus A_0 show some separation between the below and above WT populations whereas plots of f_c versus A/T show no significant separation. For a fixed yield, f_c for shots below and above WT are nearly indistinguishable whereas both A_0 and A/T are considerably larger for shots below WT than for those above WT, presumably due to improved source coupling of shots in water saturated environment. A comparison of yields estimated from A_0, A/T, A_0 combined with f_c, and A/T combined with f_c demonstrates that substantially more precise yield determinations can be made if it is known whether the shot was detonated above or below WT. Results from the analysis of 17 NTS shots recorded at the RSTN station, RSSD are generally not as well defined but appear similar to those from the JAS recordings. The largest difference between the below and above WT shots of a given yield lies in their low-frequency spectral level and, to a slightly smaller extent, in their m_b values.

Examination of m_b versus yield from large data bases of NTS shots recorded at regional and teleseismic distances also shows that, for a fixed yield, shots below WT have significantly larger m_b than those detonated above WT. Gas-filled porosity of the shot medium appears to be the dominant reason for the large magnitude bias between below and above WT shots. For shots detonated near the water table, explosion cavity and its proximity to WT can also significantly influence the source coupling. Below and above WT shots may be distinguished by comparing their Pn and Lg phases at common recording stations.

TABLE OF CONTENTS

INTRODUCTION

The geological environment in which a nuclear explosive is emplaced has a major influence on the strength of seismic signals. For example, Werth and Herbst (1963) found that for a fixed yield, the first half-cycle amplitudes for granite and salt are nearly equal, for tuff the amplitude is about one-half the amplitudes for granite and salt, and for dry alluvium the amplitude is about one-tenth the amplitudes for granite and salt. These trends were confirmed by Springer (1966) who further suggested that dry porosity is the parameter responsible for such wide variations in seismic coupling. Murphy (1981) reviewed available observed m_b/yield and free-field data from contained explosions in a variety of source media and concluded that the coupling into the teleseismic P wave transmission path is about the same for shots in granite, shale, and wet tuff-rhyolite emplacement media, whereas explosions in dry unconsolidated material couple significantly less efficiently.

Werth and Herbst (1963) noted that explosions in higher velocity rock are significantly richer in higher frequencies. Yet their data for 5 kt shots in alluvium and tuff (Figure 3, Werth and Herbst, 1963) indicate more high frequencies for alluvium than for tuff (or higher corner frequency f_c for alluvium than for tuff), together with amplitudes in tuff about 5 times larger than in alluvium. Non-linear finite difference calculations (Bache, 1982) indicate that the most important characteristic of NTS tuff is its porosity, which can account for the large observed differences in the seismic coupling of events above and below the water table. A comparison of source functions for Yucca Flat wet and dry tuff (Bache, 1982; Figure 11) shows a larger low-frequency amplitude and lower f_c for wet tuff in comparison to dry tuff, when yield values are the same. Evernden et al. (1986) also show similar strong dependence of explosion P wave spectra on the material properties of the coupling media (see especially

their Figure 8). Gupta and Blandford (1987) examined teleseismic P from shots in saturated (below water table) media and found spectral differences to depend on the shot medium velocity. It seems therefore that both amplitudes and spectral shapes are significantly influenced by the geological environment of the shot point.

In this study, the amplitude and spectra of the regional phase Pn are compared for shots detonated below and above the water table. The three parameters estimated from each record for this purpose are corner frequency f_c, low-frequency spectral level A_0, and the time-domain measurement A/T (a measure of m_b). Short-period, vertical-component data from two stations, JAS (with records from 22 shots) and RSSD (with data from 17 shots) are analyzed. The results indicate that, for a given yield, both A_0 and m_b are significantly larger for shots below WT than for those above WT, but the f_c values are not distinguishable. These results are in agreement with those derived from substantially larger data sets of both regional and teleseismic measurements.

ANALYSIS OF REGIONAL DATA RECORDED AT JAMESTOWN (JAS)

Spectral and Time-domain Measurements:

We analyzed digital data from 22 NTS shots well recorded at 20 samples/sec at the
DWWSSN station Jamestown, JAS at epicentral distances of about 350 km. Table 1 lists
these 22 explosions along with pertinent information such as the shot medium, magnitude m_b,
and whether the shot point is above or below the water table. Out of 22 shots, only 9 are
below WT; 19 shots are from the Yucca Flats and only 3 (SERPA, HARZER, and SALUT)
are from the Pahute Mesa regions of the NTS.
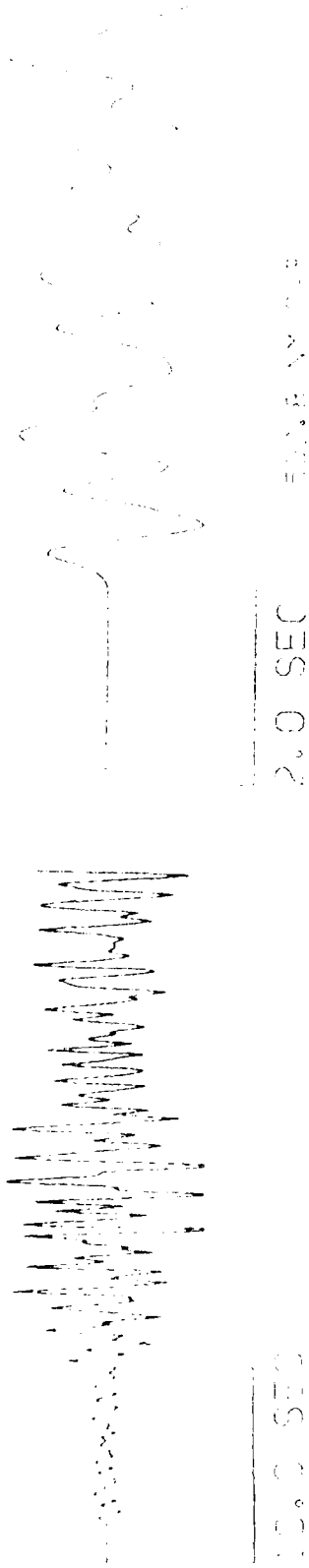
TABLE 1

NTS SHOTS RECORDED AT JAS

No.	Date	Name	Shot Medium	m_b	Gas Porosity (vol %)	Shot Depth (m)	Depth of WT (m)	Symbol[*]
1	14 Nov 1980	DAUPHIN	tuff	4.1	17.0	320	580	YO
2	17 Dec 1980	SERPA	tuff	5.1	10.0	573	627	PO
3	29 May 1981	ALIGOTE	tuff	4.2	8.0	320	605	YO
4	06 Jun 1981	HARZER	tuff	5.5	3.0	637	668	PO
5	27 Aug 1981	ISLAY	tuff	-	23.0	294	567	YO
6	01 Oct 1981	PALIZA	tuff	4.9	6.0	472	530	YO
7	11 Nov 1981	TILCI	alluvium	4.8	10.1	445	494	YO
8	12 Nov 1981	ROUSANNE	tuff	5.3	-2.0	518	495	YX
9	03 Dec 1981	AKAVI	tuff	4.6	14.3	494	580	YO
10	28 Jan 1982	JORNADA	tuff	5.9	0.0	640	507	YX
11	29 Sep 1982	BORREGO	tuff	-	0.0	564	501	YX
12	26 May 1983	FAHADA	tuff	4.4	12.0	384	600	YO
13	09 Jun 1983	DANABLU	alluvium	4.5	12.5	320	584	YO
14	22 Sep 1983	TECHADO	tuff	-	0.0	533	500	YX
15	31 May 1984	CAPROCK	tuff	5.8	0.0	600	500	YX
16	20 Jun 1984	DUORO	tuff	4.6	14.0	381	480	YO
17	02 Aug 1984	CORREO	tuff	4.7	13.0	335	470	YO
18	15 Mar 1985	VAUGHN	tuff	4.8	11.0	427	498	YO
19	12 Jun 1985	SALUT	rhyolite	5.5	4.0	698	622	PX
20	05 Dec 1985	KINIBOTO	tuff	5.7	0.0	579	488	YX
21	22 Mar 1986	GLENCOE	tuff	5.1	0.0	610	522	YX
22	14 Nov 1986	GASCON	tuff	5.8	0.0	594	508	YX

* P and Y denote Pahute Mesa and Yucca Flats regions and

O represents above and X below the water table shots

Digital, vertical component data from JORNADA and the Joint Verification Experiment (JVE) shot, KEARSARGE (17 August 1988; 37.29° N, 116.31° W) are shown in Figure 1 The JVE shot was recorded at the new DWWSSN station, CMB, about 10 km away from JAS; all available data are shown. JORNADA, detonated below WT, has m_b 5.9 which suggests a yield value close to 150 kt (see, e.g. Bache, 1982) The JVE shot, known to be above WT, also had a yield of probably close to 150 kt although its m_b is only 5.4. The large difference in the Pn amplitudes for the two shots is most probably due to the large differences

JORNADA (JAS)--BWT

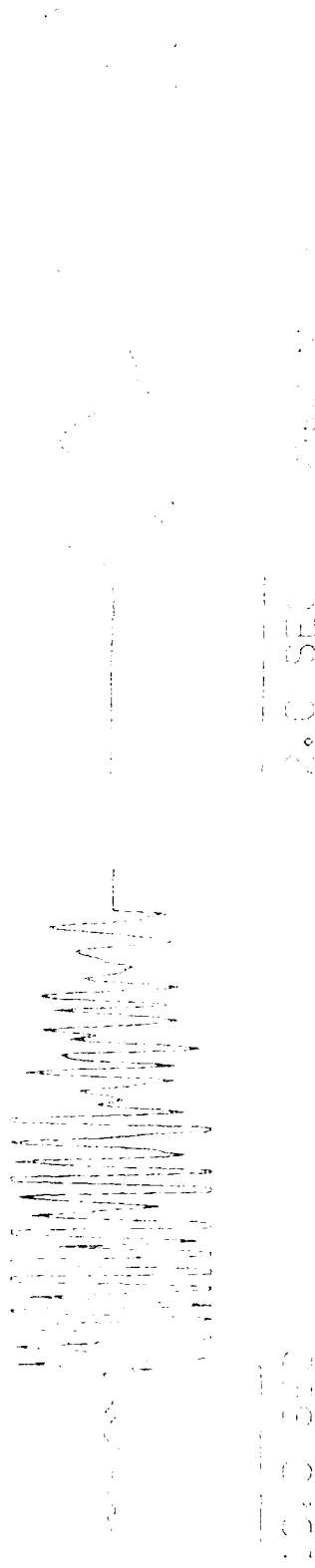2.0 SEC

KEARSARGE (CMB)--AWT

20.0 SEC

Figure 1. Short-period, vertical-component records of JORNADA (below water table) at JAS and KEARSARGE (above water table) at CMB (located within 10 km of JAS) with 2 sec of noise before the onset of Pn, with two different time scales. Note the large difference in the Pn amplitudes. Pg is clipped for both events but Pn/Pg amplitude ratio is much smaller for KEARSARGE than for JORNADA.

in coupling expected for shots below and above the WT. It is interesting to note that although Pg is clipped for both shots, the Pn/Pg amplitude ratio is much smaller for KEARSARGE than for JORNADA. In fact, a comparison of the later, unclipped portion of Pg (or Pg "coda") amplitudes appears to suggest that Pg may not show the effect of the water table.

A window length of 6.4 sec (128 points) with 10% cosine taper is used for spectral analysis of Pn. The spectra are corrected for noise by computing spectra of a window of noise prior to the onset of Pn and subtracting the power in the noise from the power in the observed signal for each discrete frequency. Examples of such spectra of the observed signal and noise, up to the Nyquist frequency of 10 Hz, are shown in Figure 2 for the same two records as in Figure 1. The spectra are without smoothing and not corrected for instrumental response. The signal-to-noise (S/N) ratio is good for almost the entire frequency range. The spectral ratio KEARSARGE/JORNADA, corrected for noise, and shown in Figure 3, has a mean slope of 0.112 per Hz (with associated standard deviation, SD of 0.004) over the frequency range of 0.2 to 6.0 Hz. Results for the frequency range of 0.2 to 10.0 Hz are also shown in the figure. The mean values of the spectral ratio (in magnitude units), integrated over the two frequency ranges by using the mean values of slope and intercept, denoted by AV INTEG in Figure 3, indicate the average spectral amplitudes in KEARSARGE to be nearly half that for JOR-NADA.

The far-field source spectra may generally be characterized by three independent parameters: the low-frequency spectral level A_0, proportional to seismic moment; the corner frequency f_c, and the power of the high-frequency asymptote (Aki and Richards, 1980). The last parameter or the value of n in f^{-n} may be assumed to be 2 for explosions (Evernden *et al.*, 1986). For explosions in same or similar media, A_0 is a good measure of the explosion yield
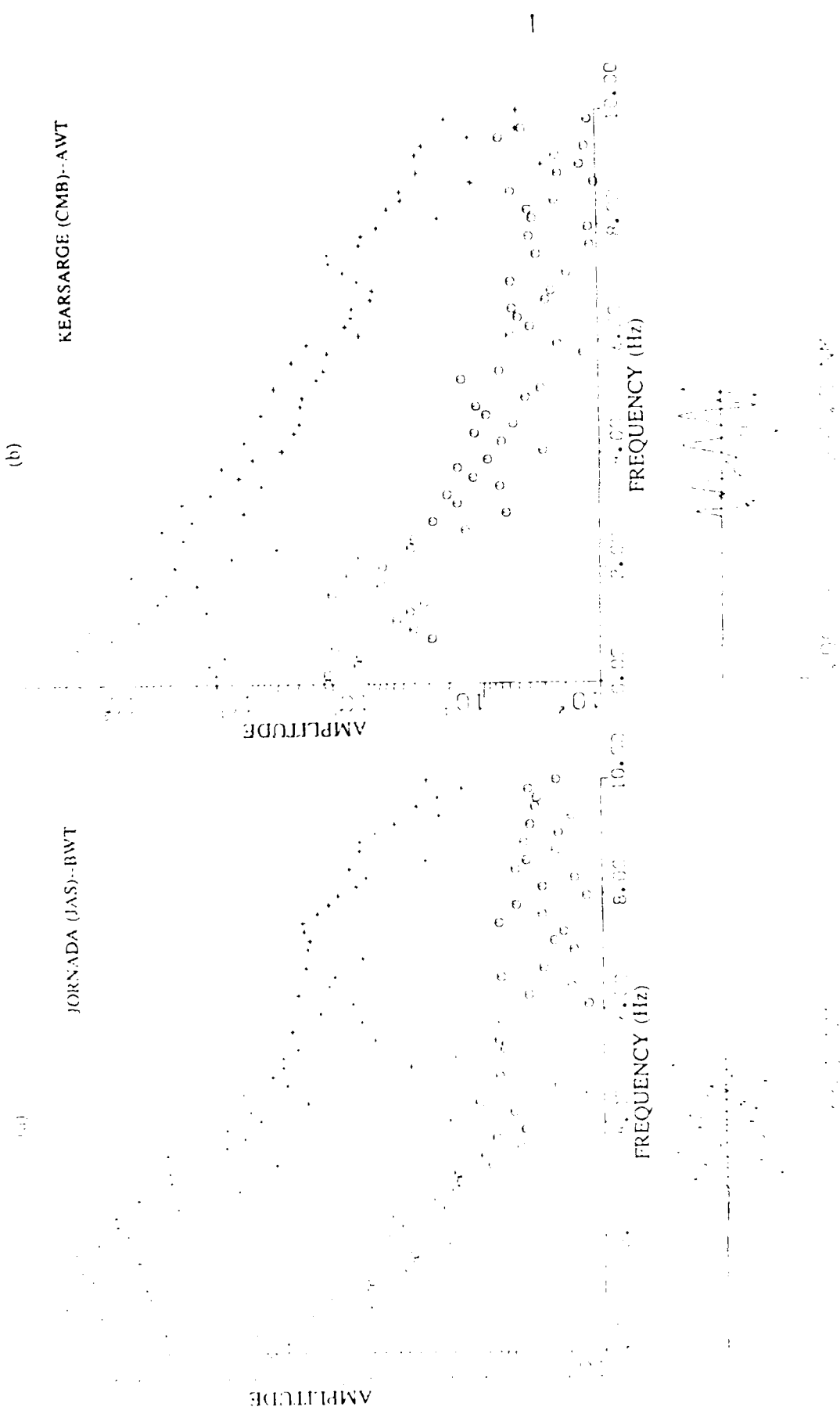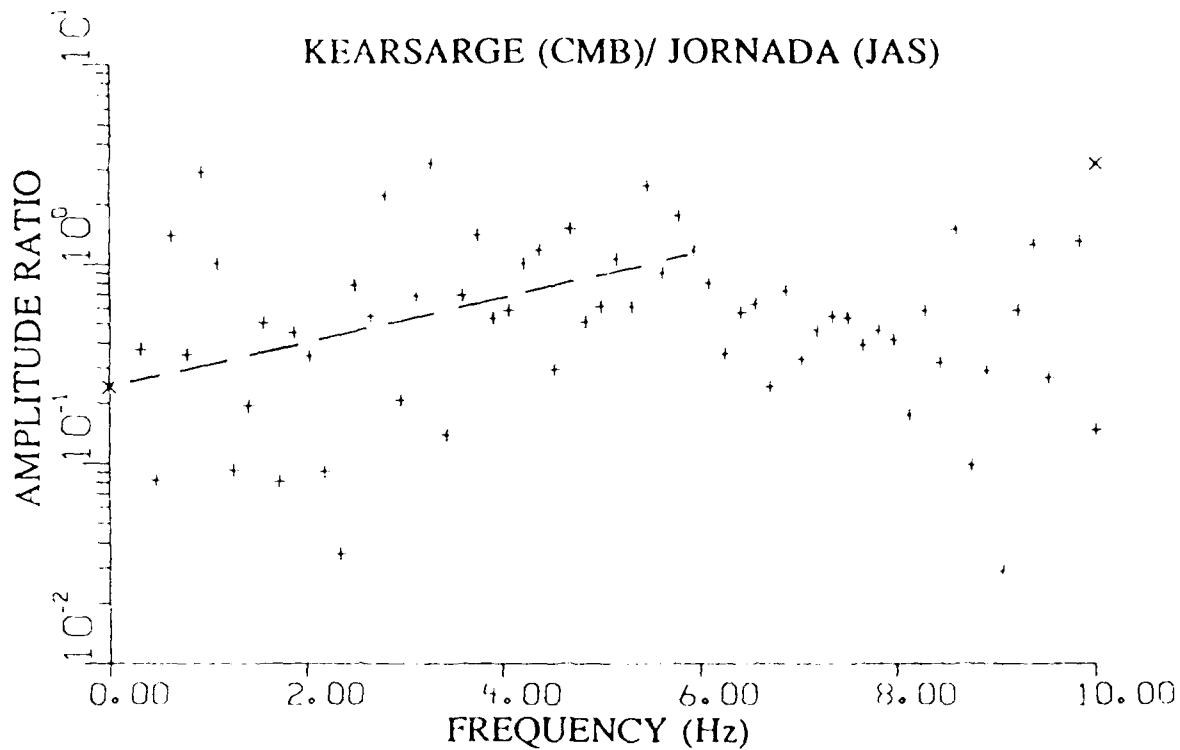
Figure 2. Vertical-component displacement amplitude spectra (symbol +) of Pn, uncorrected for instrument response and based on 6.4 sec long window with 10% cosine taper, on JAS and CMB records of JORNADA and KEARSARGE, respectively. Spectra of an equal window length of noise (symbol ˚) are also included. S/N appears good up to the Nyquist frequency of 10 Hz.

Figure 3. Spectral ratio KEARSARGE/JORNADA of Pn, corrected for noise. Points for which S/N power ratio is less than 1.5 are not plotted. The dashed line shows the mean least squares slope over the frequency range of 0.2 to 6.0 Hz. Mean slope, with associated standard deviation, SD and mean value of log amplitude ratio (AV INTEG) are indicated for two frequency ranges.

The table within the figure:

FREQ	BAND	SLOPE	S.D.	AV INTEG
0.2	6.0	0.112	0.004	-0.268
0.2	10.0	-0.001	0.002	-0.320

(Evernden *et al.*, 1986; McLaughlin *et al.*, 1987). A spectral measure of A_0 is made by correcting for noise, removing the instrument response, applying the appropriate spatial attenuation correction and then least-squares fitting the log-amplitude spectra to a model spectrum with a fall-off rate of f^{-2}. Only those data points that have S/N larger than a specified value are used in the least-squares regression. The amplitude spectrum is assumed to have the form (Brune, 1970)

$$A(f) = \frac{A_0}{1 + (f/f_c)^2}.$$ (1)

Bakun and Johnson (1970) analyzed earthquake and NTS explosion data recorded at JAS and found Q to be about 400 for Pn at regional distances. This corresponds to t^* of about 0.1 for NTS shots recorded at JAS. Applying this attenuation correction, spectral fits for JOR-NADA and KEARSARGE, based on S/N power threshold of 1.5, are shown in Figure 4 which clearly demonstrates the latter shot to have significantly lower A_0 and higher f_c than those for the former shot. The frequency range used for spectral fits was 0.2 to 6.0 Hz since most shots showed good S/N only in this frequency band.

A similar procedure was applied to all 22 shots to obtain values of A_0 and f_c, which are plotted on log-log scale in Figure 5a in which the explosion numbers correspond to those in Table 1. Below WT (denoted by X) and above WT (marked by circles) shot populations do not appear to show an obvious separation. The mean slope and intercept values are -0.245 (0.051) and 0.654 (0.104), respectively, where the quantities within parentheses denote one SD value. Data from the 9 below WT shots and the 13 above WT shots are plotted in Figures 5b and 5c, respectively. Least squares linear regressions of data in these two figures yielded mean slopes of -0.302 (0.061) and -0.283 (0.104), respectively. Both of these slope values are
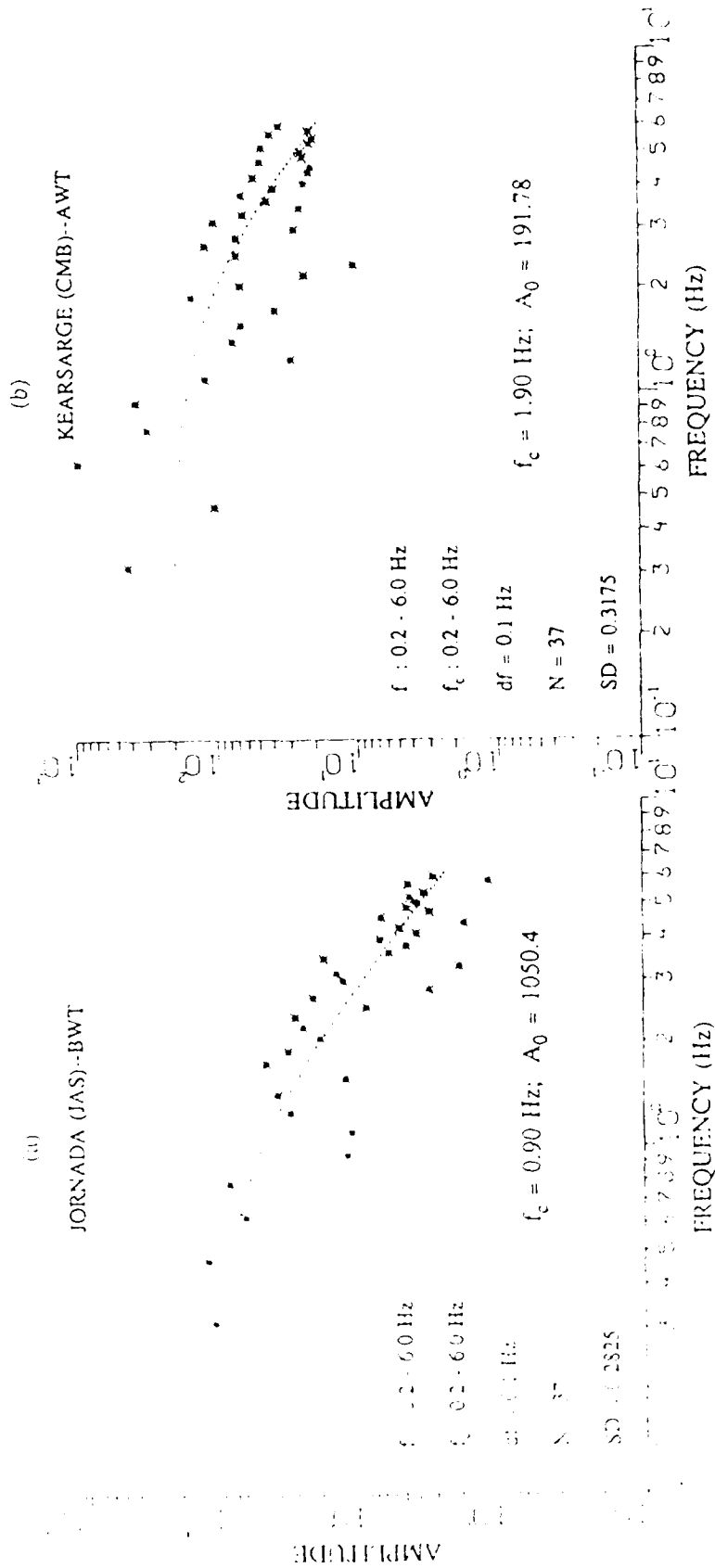
Figure 4. Displacement spectral fits of (a) JORNADA and (b) KEARSARGE for corner frequency, f_c, and low-frequency spectral level. A_0. Model spectrum (denoted by -) is a least-squares fit to the log-amplitude spectrum (denoted by *). Input parameters and the output results are listed.
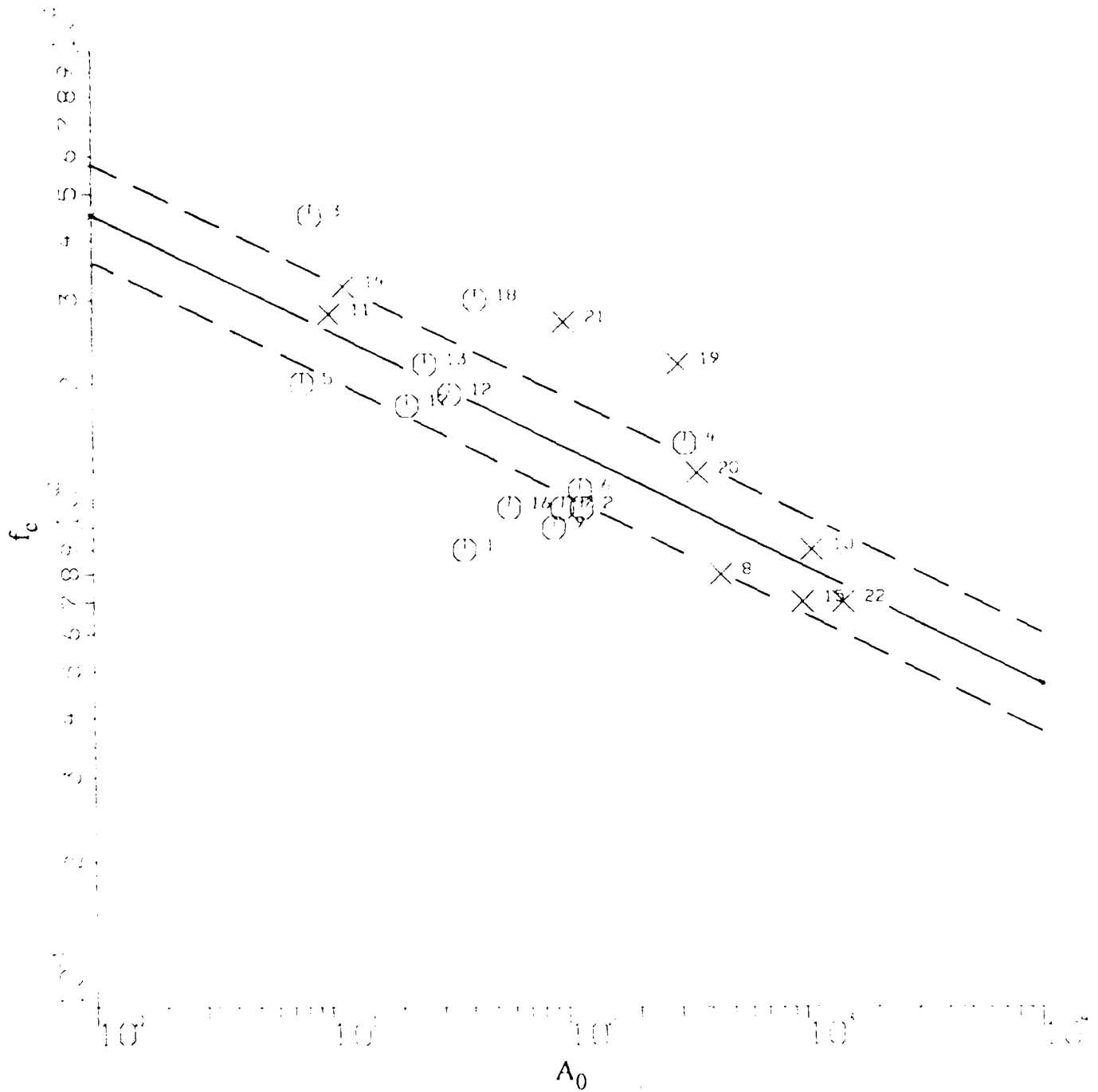
(a) JORNADA (JAS)-BWT

$f_c = 0.90$ Hz; $A_0 = 1050.4$

f : 0.2 - 6.0 Hz
f_c : 0.2 - 6.0 Hz
df = 0.1 Hz
N = 37
SD = 0.2825

(b) KEARSARGE (CMB)-AWT

$f_c = 1.90$ Hz; $A_0 = 191.78$

f : 0.2 - 6.0 Hz
f_c : 0.2 - 6.0 Hz
df = 0.1 Hz
N = 37
SD = 0.3175

Figure 5a. f_c versus A_0 for 9 below water table (denoted by X) and 13 above water table (marked by circles) shots numbered as in Table 1 and based on $t^* = 0.1$. The least squares linear regression through all 22 data points (continuous line) has correlation coefficient of 0.731, slope of -0.245, and intercept of 0.654. One SD variation in the intercept value is shown by the dashed lines.
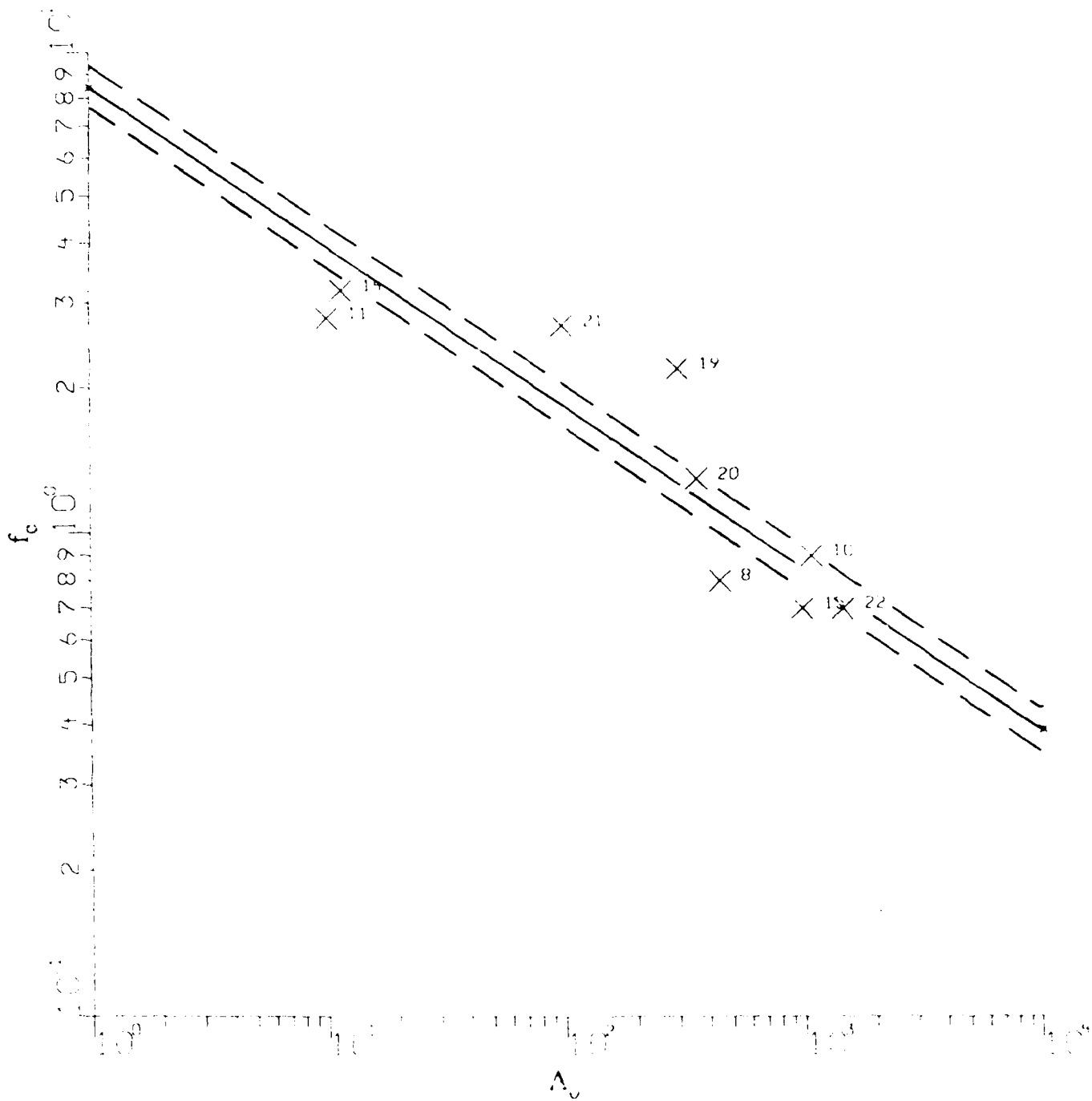
11

Figure 5b. Similar to Figure 5a for only 9 below water table shots. Forcing a slope of -1/3, the least squares linear regression (continuous line) has an intercept of 0.926.
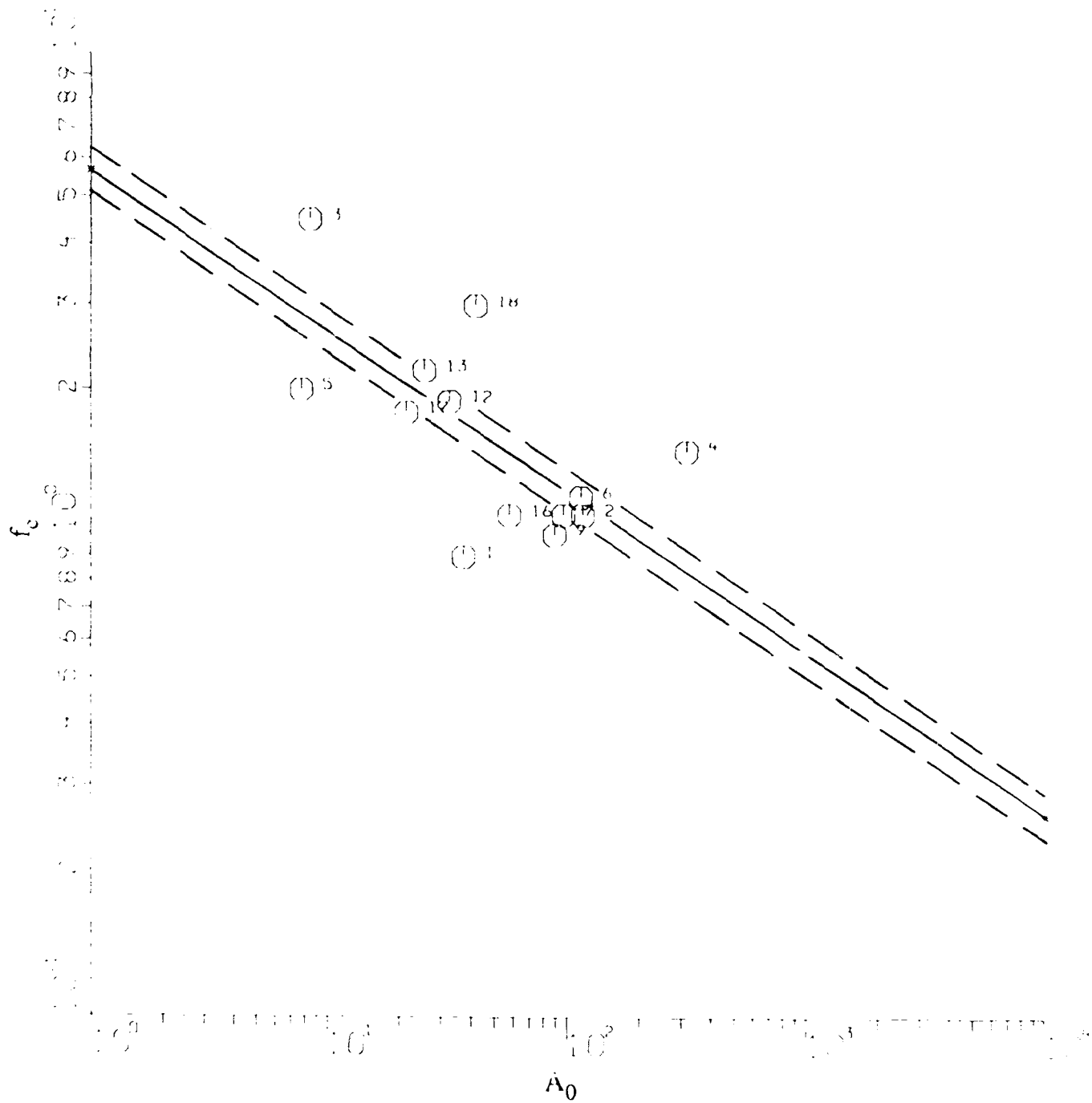
Figure 5c. Similar to Figure 5a for only 13 above water table shots. Forcing a slope of -1/3, the least squares linear regression (continuous line) has an intercept of 0.754.

within one SD of the theoretically expected value of -1/3. We therefore forced a slope of -1/3 through the data points in Figures 5b and 5c and the least squares regressions gave mean intercept values of 0.926 (0.044) and 0.754 (0.045), respectively. Thus the below and above WT populations are separated by 0.172 (0.063). In other words, for the same low-frequency spectral level, shots below WT have, on the average, larger (about a factor of 1.5) f_c than those above WT.

Determination of f_c is obviously dependent on the attenuation relationship assumed in correcting the observed amplitudes. A different attenuation correction is therefore tried in order to examine how the results pertaining to below and above WT shot populations are affected. Analyzing Pn spectra of a large number of NTS shots recorded at regional distances, Taylor et al. (1987) suggested the following frequency-dependent attenuation relationship:

$$Q = 250 \, f^{0.6} \tag{2}$$

This correction is applied to the data by assuming a propagation velocity of 8 km/sec for Pn. The resulting plots of A_0 versus f_c are shown in Figures 6a, 6b, and 6c for all (22) shots, 9 shots below WT, and 13 shots above WT, respectively. The mean slope and intercept values for all shots (Figure 6a) are -0.237 (0.042) and 0.497 (0.098), respectively. The mean slope values for the data in Figures 6b and 6c are -0.276 (0.055) and -0.272 (0.087), respectively; both of these slope values are within one SD of the theoretically expected value of -1/3. A slope of -1/3 is therefore forced through the data points in Figures 6b and 6c and the least squares regressions give mean intercept values of 0.802 (0.044) and 0.648 (0.039), respectively. Thus the below and above WT populations are separated by 0.154 (0.059). This result is very nearly the same as obtained earlier based on $t^* = 0.1$. It means that the separation
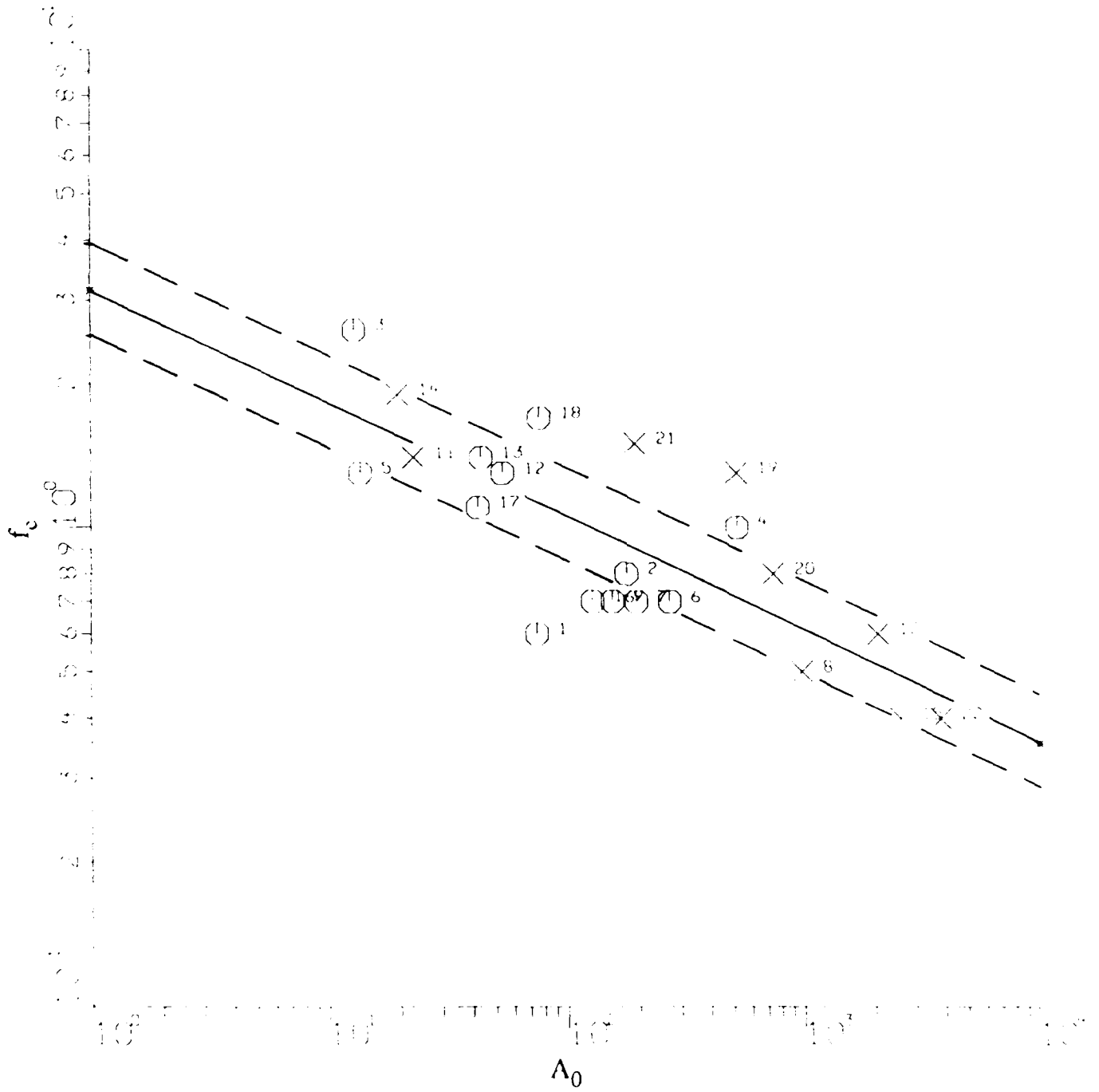
14

Figure 6a. Similar to Figure 5a but based on frequency-dependent Q. The least squares linear regression (continuous line) has correlation coefficient of 0.782, slope of -0.237, and intercept of 0.497.

Figure 6b. Similar to Figure 6a for only 9 below water table shots. Forcing a slope of -1/3, the least squares linear regression (continuous line) has intercept of 0.802.
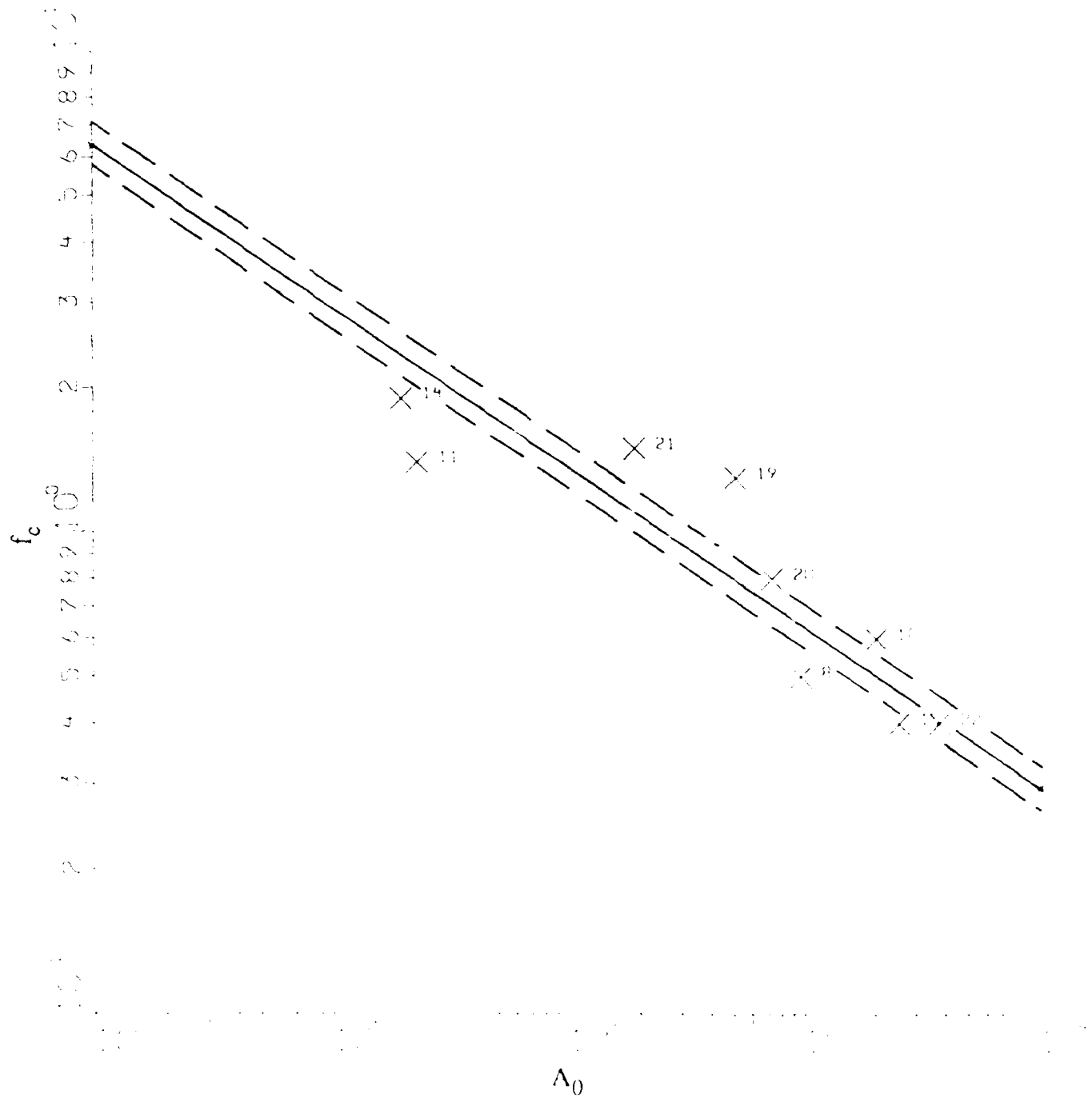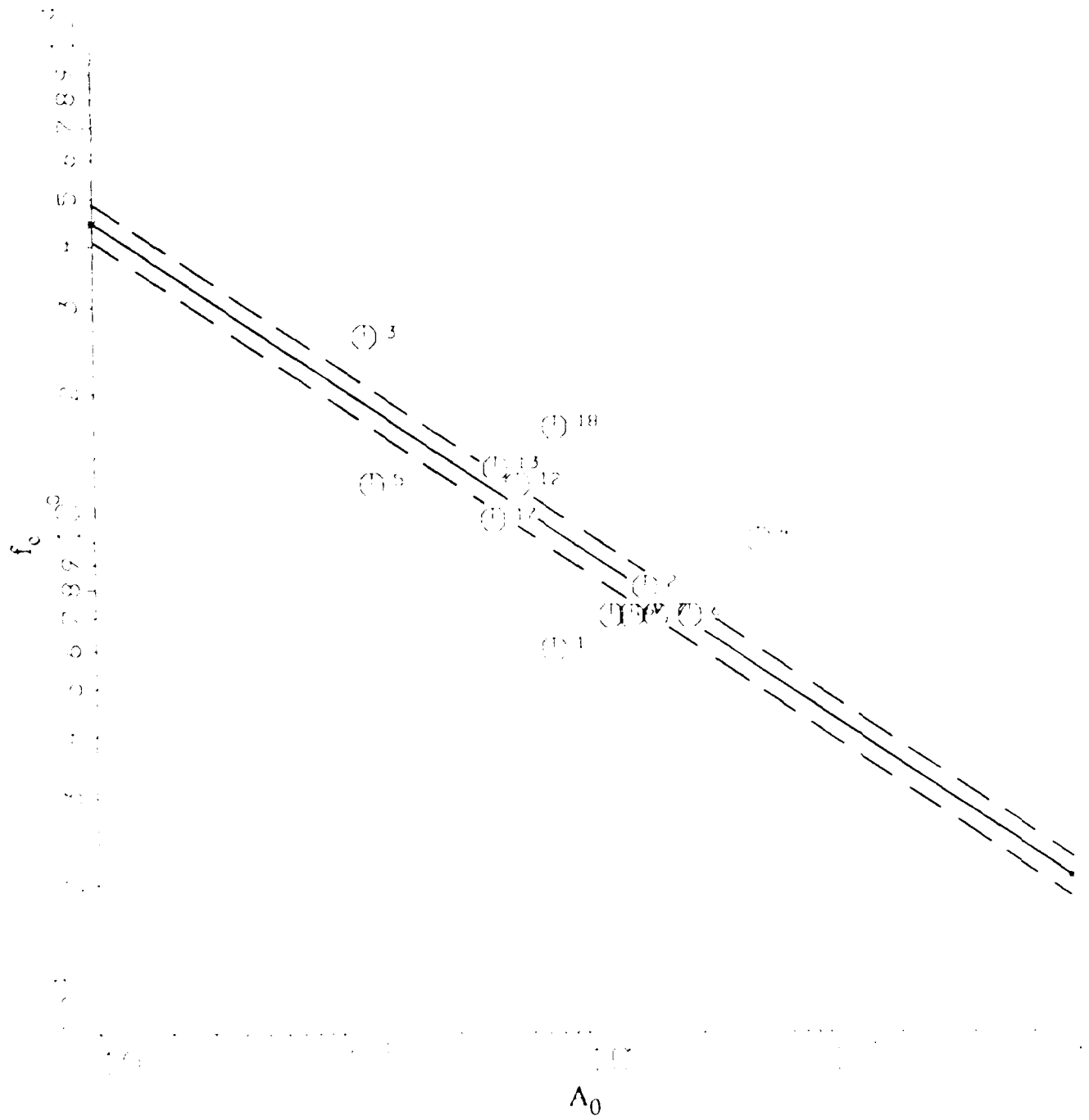
Figure 6c. Similar to Figure 6a for only 13 above water table shots. Forcing a slope of -1/3, the least squares linear regression (continuous line) has intercept of 0.648.

between below and above WT populations is not much influenced by the choice of attenuation model and is therefore significant.

Note that as far as the distinction between below and above WT shots is concerned, the results based on $t^* = 0.1$ (Figures 5a, b, c) and those based on frequency-dependent Q (Figures 6a, b, c) are nearly identical; the relative distribution of various data points is almost the same for the two sets of figures and only the mean intercept values are different. Also the separation between the below and above WT populations is nearly independent of the attenuation model used for correcting Pn amplitudes. For this reason, subsequent analyses of data are restricted to the use of only one attenuation model, viz. $t^* = 0.1$.

Time domain measurements of A/T are also made on all 22 JAS records. Plots of f_c (derived by assuming $t^* = 0.1$) versus log A/T are shown in Figures 7a, 7b, and 7c for all (22) shots, below WT (9) shots, and above WT (13) shots, respectively. The mean slope values for the data in these three figures are -0.220 (0.080), -0.296 (0.110), and -0.149 (0.164), respectively. When the mean slope derived from the entire data set (viz. -0.220) is forced through the data points in Figures 7b and 7c, the mean intercept values are 0.714 (0.067) and 0.654 (0.056), respectively. Thus, for a given A/T or m_b value, f_c values for shots below and above WT are not significantly different.

Plots of f_c versus yield (on log-log scale) for all shots showed mean slope and intercept values of -0.249 (0.070) and 0.541 (0.109), respectively. For below WT and above WT shots, the mean slopes were -0.247 (0.093) and -0.249 (0.138), respectively. Both of these slope values are within one SD of the theoretically expected value of -1/3. A slope of -1/3 was therefore forced through the data points and the least squares regressions gave mean intercept

18
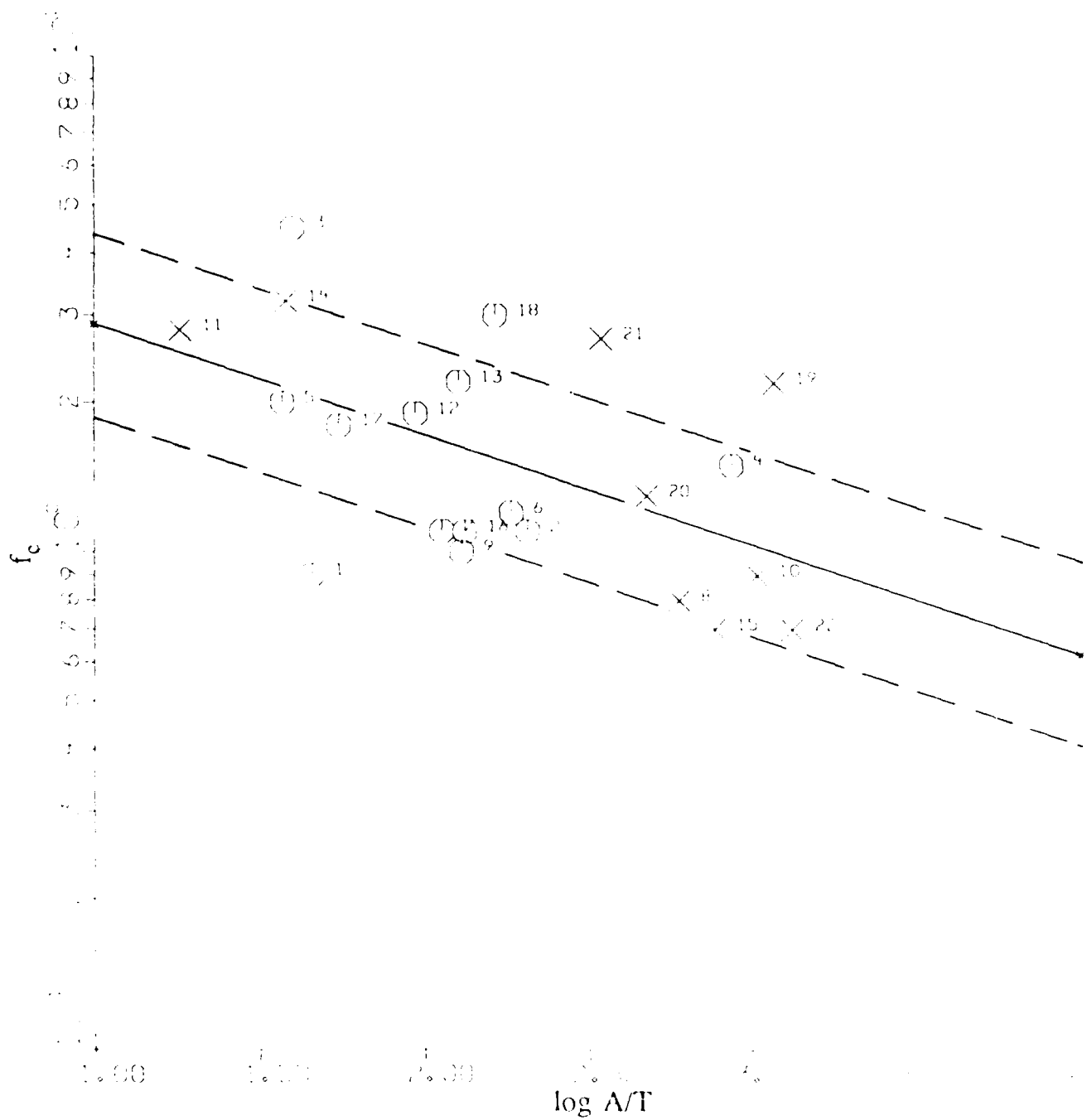
Figure 7a. f_c versus log A/T for 9 below water table (denoted by X) and 13 above water table (marked by circles) shots based on $t^* = 0.1$. The least squares linear regression through all 22 data points (continuous line) has correlation coefficient of 0.524, slope of -0.220, and intercept of 0.678. One SD variation in the intercept value is shown by the dashed lines.

19

Figure 7b. Similar to Figure 7a for only 9 below water table shots. Forcing a slope of -0.220, the least squares linear regression (continuous line) has intercept of 0.714.

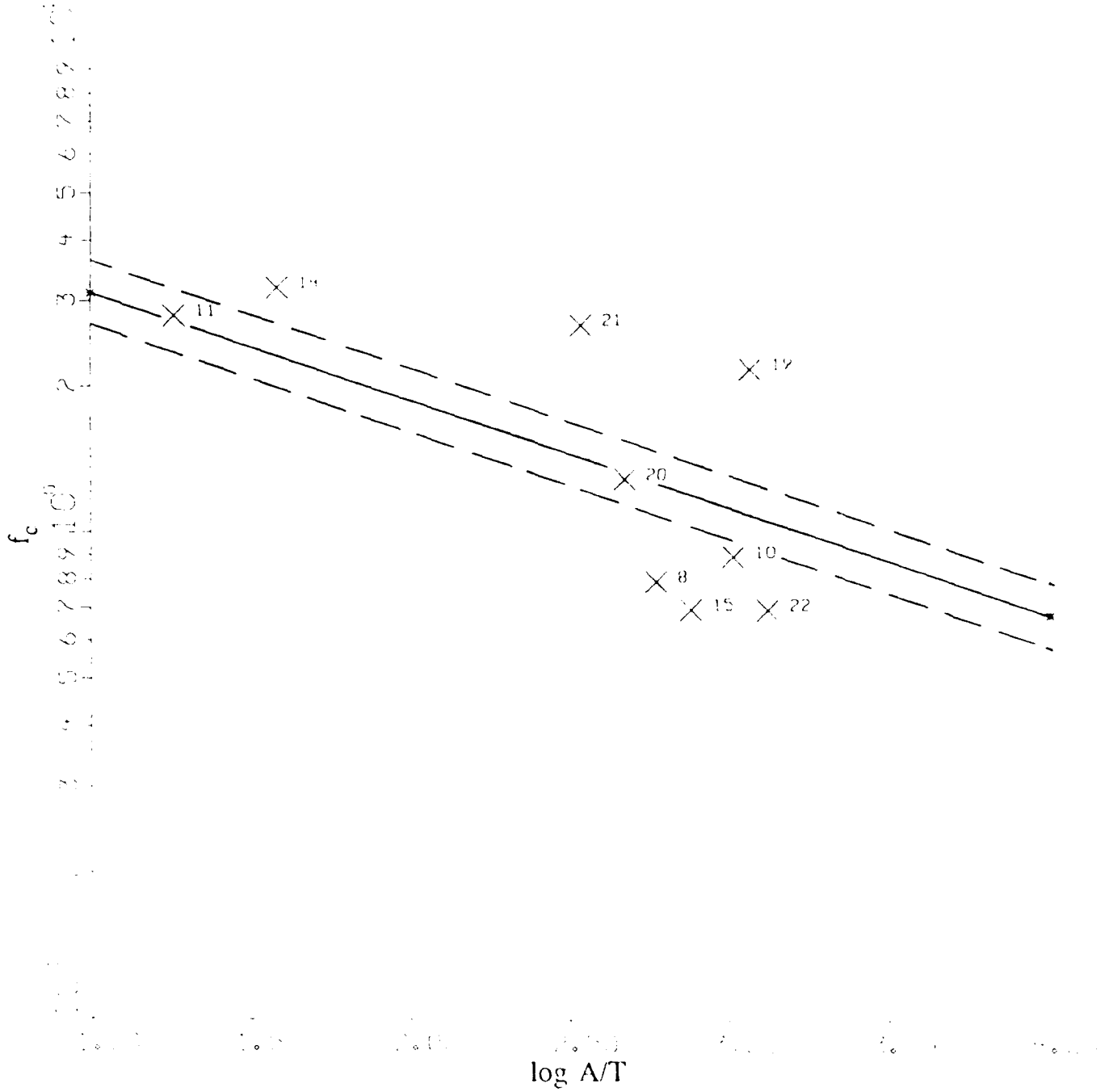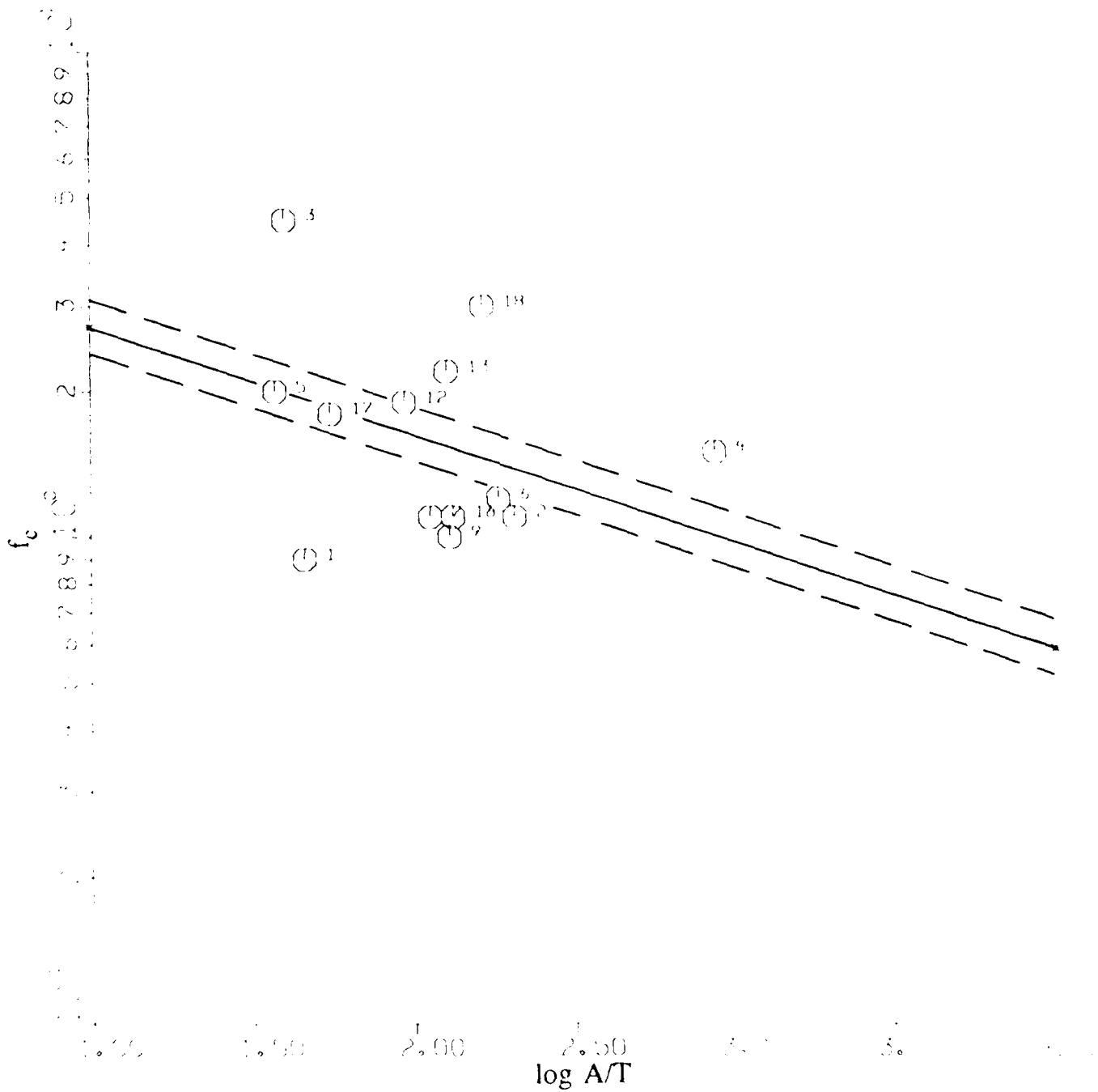Figure 7c. Similar to Figure 7a for only 13 above water table shots. Forcing a slope of -0.220, the least squares linear regression (continuous line) has intercept of 0.654.

values of 0.663 (0.069) and 0.662 (0.051), respectively. Thus there is no separation between the below and above WT populations. In other words, for a fixed yield, f_c values for shots below and above WT are not significantly different.

Plots of A_0 versus yield (on log-log scale) for all (22) shots, below WT (9) shots, and above WT (13) shots gave mean slopes of 1.061 (0.124), 0.969 (0.118), and 1.094 (0.119), respectively. All of these slope values are within one SD of the theoretically expected value of 1. When a slope of 1 was forced through the data points, the least squares regressions give mean intercept values of 0.789 (0.083) and 0.276 (0.045), respectively. Thus the below and above WT populations are separated by 0.513 (0.095). In other words, for the same value of yield, A_0 for a shot below WT is, on the average, significantly larger (about a factor of 3) than that for a shot above WT.

Plots of log A/T versus yield for all shots, below WT shots, and above WT shots gave mean slopes of 0.875 (0.086), 0.829 (0.048), and 0.846 (0.111), respectively. When the mean slope derived from the entire data set (viz. 0.875) was forced through the data points, the mean intercept values were 1.206 (0.036) and 0.844 (0.041), respectively. Thus, the below and above WT populations are separated by 0.362 (0.0542). In other words, for a fixed yield, log A/T or m_b for a shot below WT is significantly larger (about 0.36 magnitude unit) than that for a shot above WT.

Yield Estimation:

In order to assess the effect of the water table on yield estimates, we computed estimated yields ($\hat{Y}$) based on A_0, A/T, A_0 and f_c, and A/T and f_c. The coefficients used to compute the estimates are first determined through linear or multilinear regressions, with the known yield

(Y) as the dependent variable:

$$\log Y = a_1 + b_1 \log A_0 \tag{3a}$$

$$\log Y = a_2 + b_2 \log A/T \tag{3b}$$

$$\log Y = a_3 + b_3 \log A_0 + c_3 \log f_c \tag{3c}$$

$$\log Y = a_4 + b_4 \log A/T + c_4 \log f_c \tag{3d}$$

Regression coefficients as well as the estimated yields ($\hat{Y}$) for each shot (along with its associated SD) are computed for 9 events below the water table (a_i^{bwt}, b_i^{bwt}, c_i^{bwt}), for 13 events above the water table (a_i^{awt}, b_i^{awt}, c_i^{awt}), and for all (22 shots) of the data together (a_i^{all}, b_i^{all}, c_i^{all}). The regression results based on log Y as the dependent variable are listed in Table 2 in which the SD of the estimated yield (in magnitude units) is denoted by s.

TABLE 2

LINEAR REGRESSION COEFFICIENTS FOR JAS DATA

Data Set	d^*	Constant a	Independent Variable	Coefficient b	Independent Variable	Coefficient c	s
ALL(22)	20	0.014		0.740			0.276
BWT(9)	7	-0.638	$\log A_0$	0.935			0.261
AWT(13)	11	0.040		0.809			0.141
ALL(22)	20	-0.718		0.958			0.239
BWT(9)	7	-1.469	$\log A/T$	1.178			0.129
AWT(13)	11	-0.663		0.995			0.165
ALL(22)	19	-0.081		0.776		0.145	0.282
BWT(9)	6	-2.095	$\log A_0$	1.451	$\log f_c$	1.707	0.115
AWT(13)	10	-0.211		0.915		0.374	0.132
ALL(22)	19	-0.391		0.852		-0.482	0.224
BWT(9)	6	-1.446	$\log A/T$	1.171	$\log f_c$	-0.025	0.139
AWT(13)	10	-0.414		0.923		-0.490	0.136

* d denotes degrees of freedom

In order to assess the improvement in yield estimates obtained by considering events above the water table separately from events below the water table, we computed two sets of estimated yields using the coefficients in Table 2. The first set is computed using the regression coefficients obtained for all of the data together, e.g.,

$$\log \hat{Y}_j = a_1^{all} + b_1^{all} (\log A_0)_j \tag{4}$$

The second set of yield estimates is computed by applying separate regression coefficients to events below and above the water table, e.g.,

$$\log \hat{Y}_j^{bwt} = a_1^{bwt} + b_1^{bwt} (\log A_0)_j^{bwt} \tag{5a}$$

$$\log \hat{Y}_j^{awt} = a_1^{awt} + b_1^{awt} (\log A_0)_j^{awt} \tag{5b}$$

Since the coupling is generally significantly smaller for events above the water table, it is likely that the second set of estimated yields (equations 5a and 5b) would be more precise, since different relationships for events below and above the water table are used, thus accounting for the coupling differences. When separate coefficients for below and above WT shots are used, the SD of $\log \hat{Y}$, S is given by

$$S^2 = \frac{d_1 s_1^2 + d_2 s_2^2}{d_1 + d_2} \tag{6}$$

where s_1, s_2 are the SD for below and above WT shots and d_1, d_2 are the corresponding degrees of freedom (see Table 2).

Consider, as an example, plots of estimated yield based on A_0. When the regression coefficients for the entire data set are used, the yield estimates for events below the water table are positively biased whereas the estimates for events above the water table are negatively biased and the SD of the estimated yield is 0.276 (Table 2). However, when separate

sets of coefficients are used, the systematic biases are eliminated and, using equation (6), the SD reduces to 0.196. Furthermore, the correlation coefficient of estimated yield with known yield improves from 0.886 to 0.950 and the slope increases from 0.785 to 0.902. A similar improvement is obtained for yield estimated from A/T, A_0 and f_c, and A/T and f_c. These improvements are summarized in Table 3 below.

TABLE 3

COMPARISON OF REGRESSION RESULTS

Estimation Parameters	Slope		Correlation Coefficient		SD of log $\dot{Y}$	
	Same Coefficients	Separate Coefficients	Same Coefficients	Separate Coefficients	Same Coefficients	Separate Coefficients
A_0	0.785	0.902	0.886	0.950	0.276	0.196
A/T	0.838	0.941	0.916	0.970	0.239	0.152
A_0, f_c	0.787	0.964	0.887	0.982	0.282	0.126
$A/T, f_c$	0.866	0.958	0.930	0.979	0.224	0.137

At least some of this increase in slope and correlation coefficient is probably due to the additional degrees of freedom, i.e., the use of twice as many regression coefficients in equation (5a) or (5b) as in equation (4). Nevertheless, a comparison of the SD values in Table 3 shows that substantially better yield estimates can be obtained if one can determine whether the event occurred above or below the water table.

Using KEARSARGE as an example, the derived values of A_0 and f_c (indicated on Figure 4) and the regression coefficients in Table 2 for above WT shots lead to the estimated yield value, $\dot{Y}$ given by

$$\log \dot{Y} = -0.211 + 0.915 (\log 191.78) + 0.374 (\log 1.9) \tag{7}$$

25

which gives a value of 96 kt. The use of only one independent variable (viz. A_0) will provide a value of 77 kt. Similarly, use of regression coefficients for all data lead to yield estimates of 50 and 54 kt when results with one (viz. A_0) and two (viz. A_0 and f_c) independent variables, respectively are used. As expected, the first value (96 kt) is a better estimate than the other three values.

RESULTS FROM THE RSTN STATION, RSSD

Short-period, vertical component, digital data from 17 NTS explosions, well recorded at the RSTN station, RSSD (40 samples/sec), with epicentral distances of about 1300 km, are also analyzed in the same manner as the JAS data. These shots are listed in Table 4; note that 10 shots are common with Table 1.

TABLE 4

NTS SHOTS RECORDED AT RSSD

No.	Date		Name	Lat	Lon	shot medium	mb	symbol*
1	1982028	28 jan 82	JORNADA	37.09	-116.05	tuff	5.9	X
2	1982175	24 jun 82	NEBBIOLO	37.24	-116.37	rhyolite	5.6	O
3	1982217	05 aug 82	ATRISCO	37.08	-116.01	tuff	5.7	X
4	1982344	10 dec 82	MANTECA	37.03	-116.07	alluvium	4.6	O
5	1983104	14 apr 83	TORQUOISE	37.07	-116.05	tuff	5.7	X
6	1983125	05 may 83	CROWDIE	37.01	-116.09	alluvium	4.5	O
7	1983146	26 may 83	FAHADA	37.10	-116.01	tuff	4.4	O
8	1983160	09 jun 83	DANABLU	37.16	-116.09	alluvium	4.5	O
9	1984091	31 mar 84	AGRINI	37.15	-116.08	alluvium	4.1	O
10	1984152	31 may 84	CAIROCK	37.10	-116.05	tuff	5.8	X
11	1984172	20 jun 84	DUORO	37.00	-116.04	tuff	4.6	O
12	1984215	02 aug 84	CORREO	37.02	-116.01	tuff	4.7	O
13	1985074	15 mar 85	VAUGHN	37.06	-116.05	tuff	4.8	O
14	1985122	02 may 85	TOWANDA	37.25	-116.33	tuff	5.7	X
15	1985163	12 jun 85	SALUT	37.25	-116.49	rhyolite	5.5	X
16	1985339	05 dec 85	KINIBOTO	37.05	-116.05	tuff	5.7	X
17	1986318	14 nov 86	GASCON	37.10	-116.05	tuff	5.8	X

* O represents above and X below the water table

Spectra of Pn (window length 6.4 sec) from ATRISCO and NEBBIOLO, two shots of similar magnitudes but the first below WT and the other above WT, are shown in Figure 8. The spectra are not smoothed and are not corrected for instrumental response. The S/N is good up to about 5 Hz. The attenuation correction for the RSSD data is assumed to be t^* =
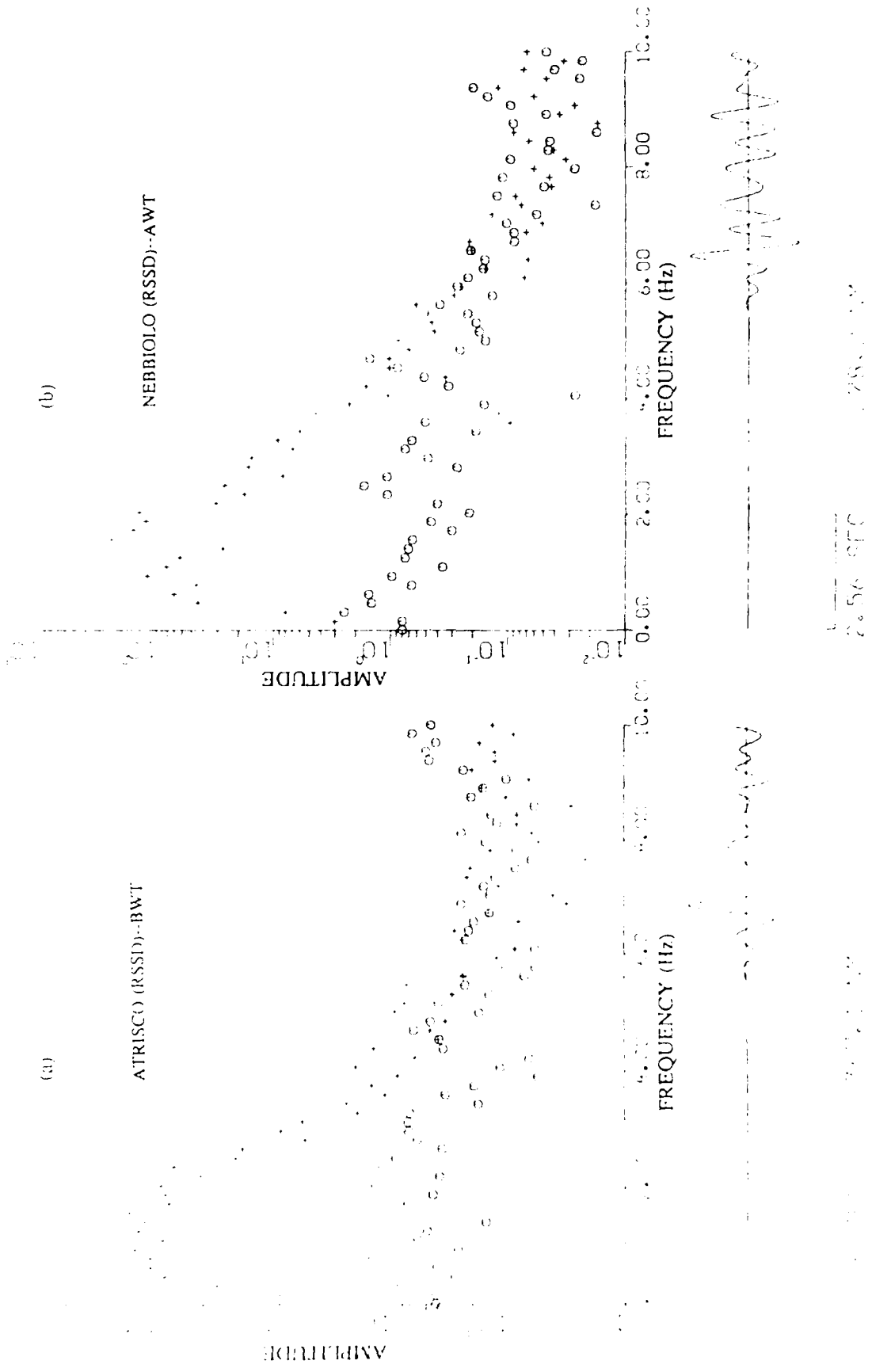
Figure 8. Vertical-component displacement amplitude spectra of Pn (6.4 sec long window), similar to those in Figure 2, for ATRISCO (below water table) and NEBBIOLO (above water table) recorded at RSSD. S/N appears good up to about 5 Hz only.

28

0.4 as the source-receiver distance is about 4 times that for the station JAS. The correspond-ing displacement spectral fits and the derived values of f_c and A_0 are shown in Figure 9. Note that f_c for the above WT shot is considerably higher than for the below WT shot, similar to the result in Figure 4.

A plot of f_c versus A_0 for all 17 shots recorded at RSSD is shown in Figure 10a; the explosion numbers correspond to those in Table 4. The mean slope and intercept values are -0.398 (0.038) and 1.071 (0.090), respectively. When the mean slope derived from the entire data set is forced on the below WT data alone (Figure 10b), the mean intercept value is 1.065 (0.032) whereas the corresponding result for only above WT shots (Figure 10c) is 1.076 (0.044). Thus there is hardly any separation between the below and above WT populations.

Time-domain measurements of log A/T, a measure of m_b, are made in the same manner as for the JAS recordings. Plots of f_c versus log A/T are shown in Figures 11a, b, and c for all (17) shots, 8 below WT shots, and 9 above WT shots, respectively. Forcing the mean slope of -0.480 obtained from the entire data set (Figure 11a), the intercept values for below and above WT populations are 1.102 (0.058) and 1.189 (0.057), respectively. Therefore, the corner frequencies for a given m_b for shots below and above WT are not significantly different.

A plot of A_0 versus yield (on log-log scale) for all 17 shots indicated the mean slope of 1.648, considerably larger than the theoretically expected value of 1 or the observed value of close to 1 for the JAS data. One reason for this is the lack of sufficient overlap in the yield values of below and above WT shots. Forcing a slope of 1 to the data points, the mean inter-cept values for all (17) shots, 8 below WT, and 9 above WT shots were 0.596 (0.103), 0.954 (0.114), and 0.278 (0.058), respectively. The below and above WT populations are therefore
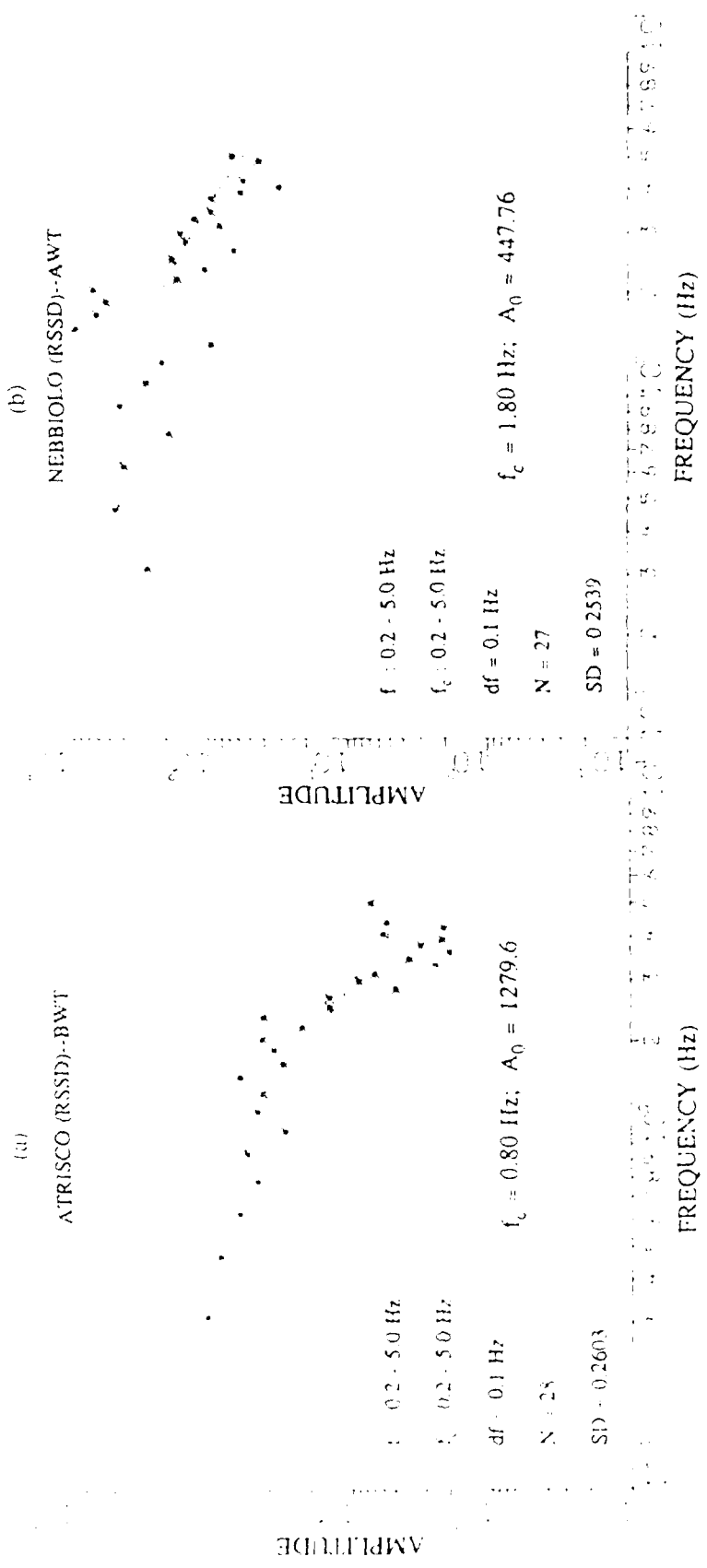
Figure 9. Displacement spectral fits of (a) ATRISCO and (b) NEBBIOLO recorded at RSSD for corner frequency, f_c, and low-frequency spectral level, A_0, similar to those in Figure 4.
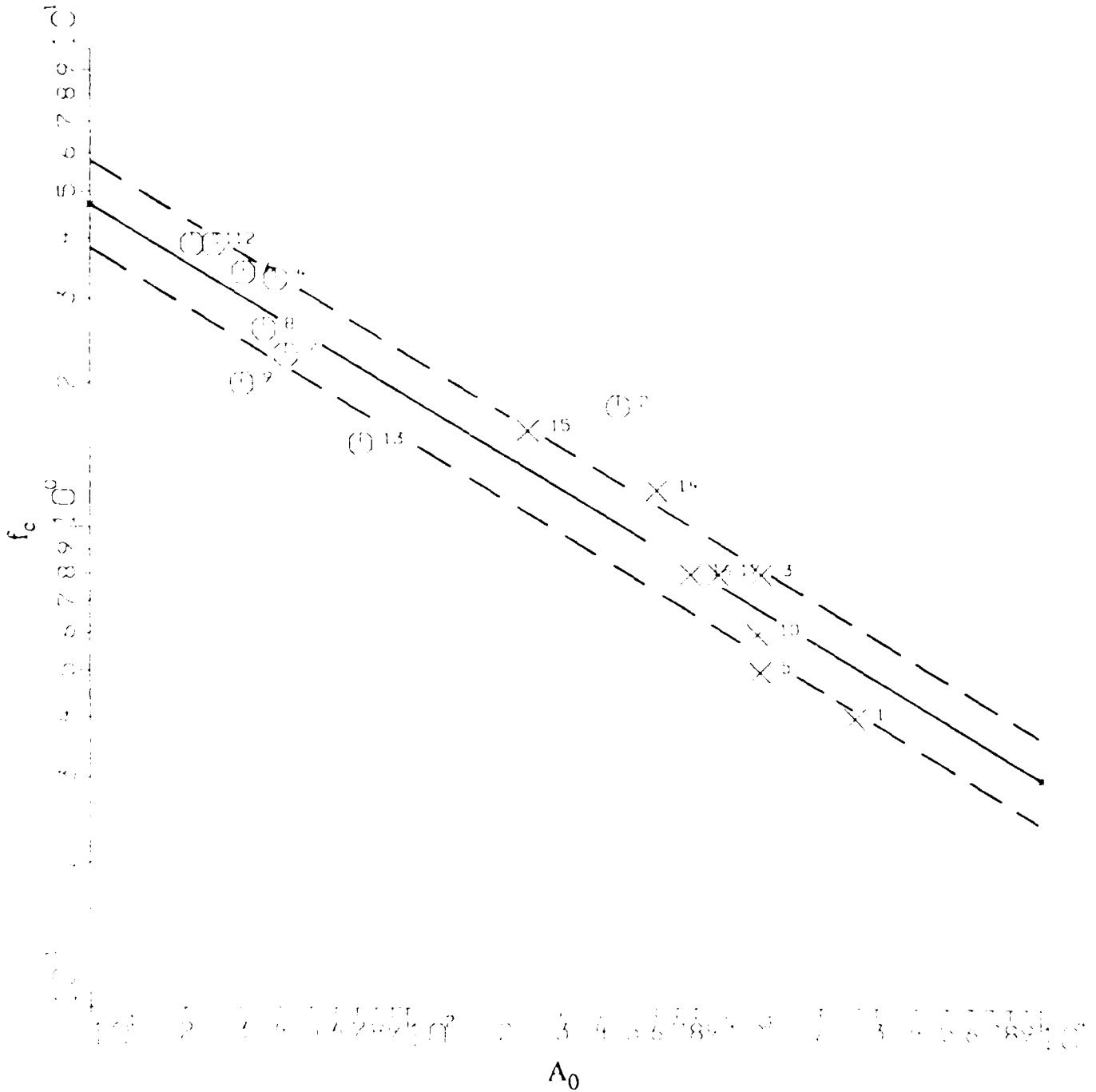
Figure 10a. f_c versus A_0 for 8 below water table (denoted by X) and 9 above water table (marked by circles) shots numbered as in Table 4 and based on $t^* = 0.4$. The least squares linear regression through all 17 data points (continuous line) has correlation coefficient of 0.939, slope of -0.398, and intercept of 1.071. One SD variation in the intercept value is shown by the dashed lines.
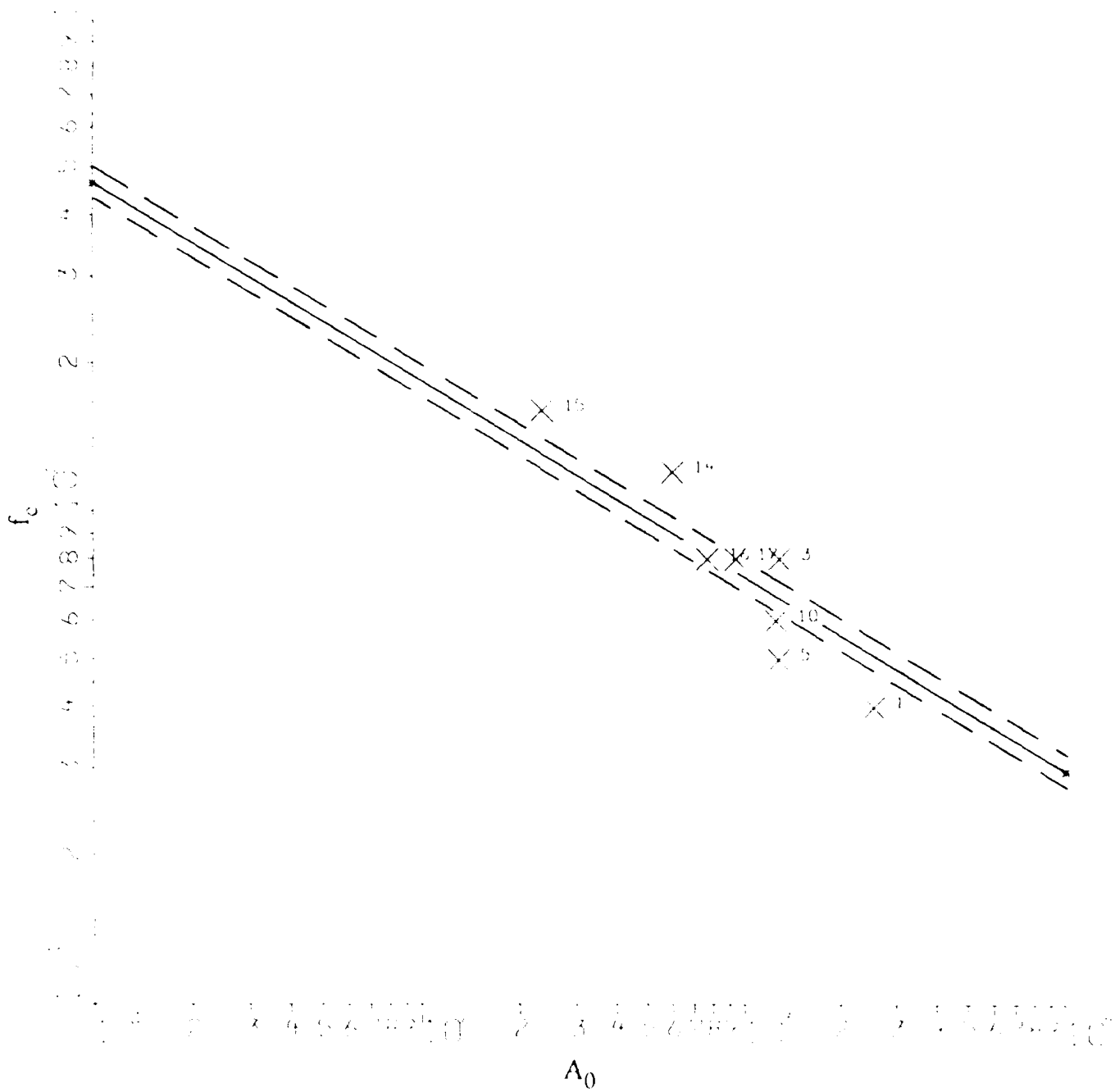
Figure 10b. Similar to Figure 10a for only 8 below water table shots. Forcing a slope of -0.398, the least squares linear regression (continuous line) has intercept of 1.065.
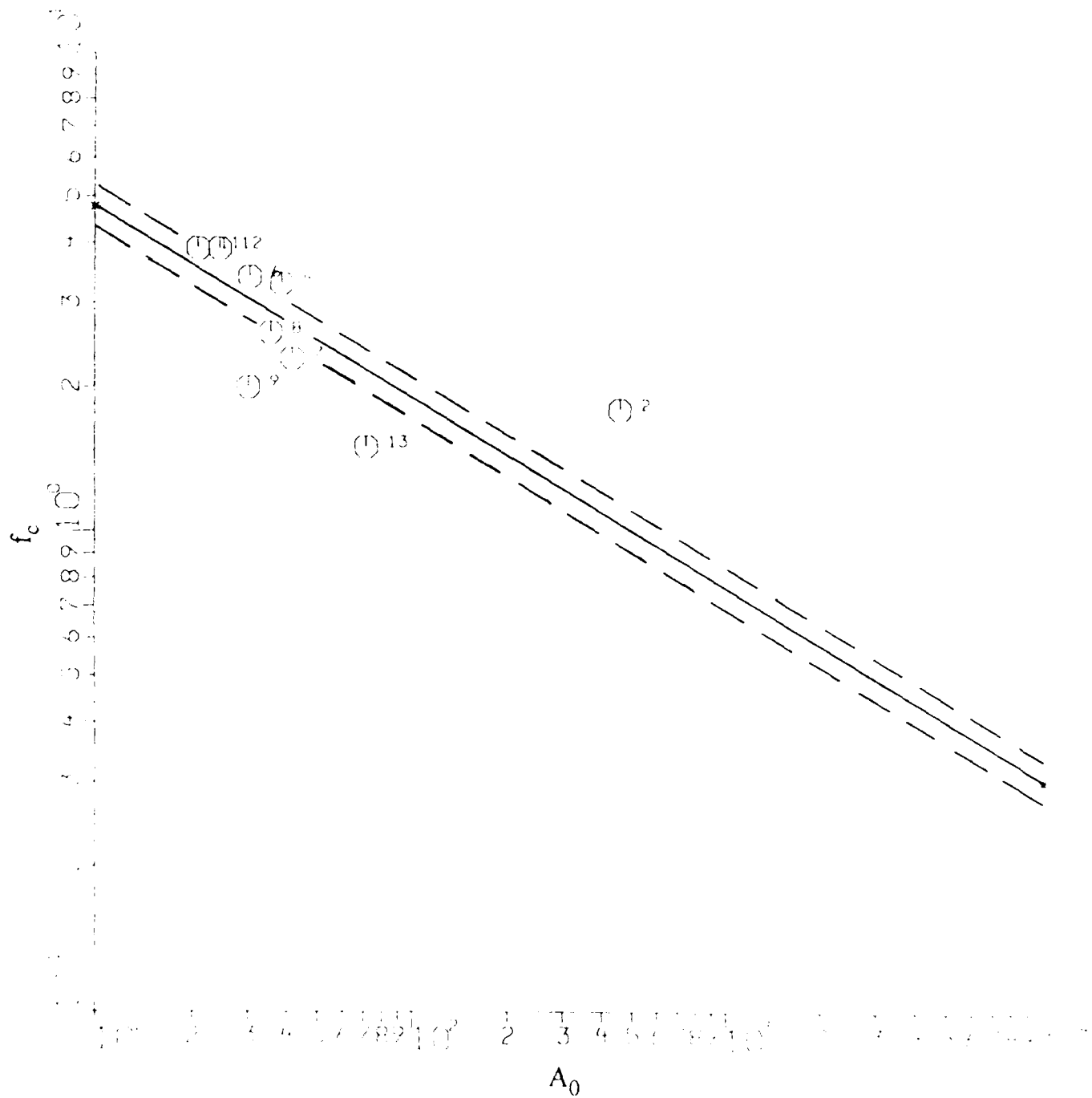
Figure 10c. Similar to Figure 10a for only 9 above water table shots. Forcing a slope of -0.398, the least squares linear regression (continuous line) has intercept of 1.076.
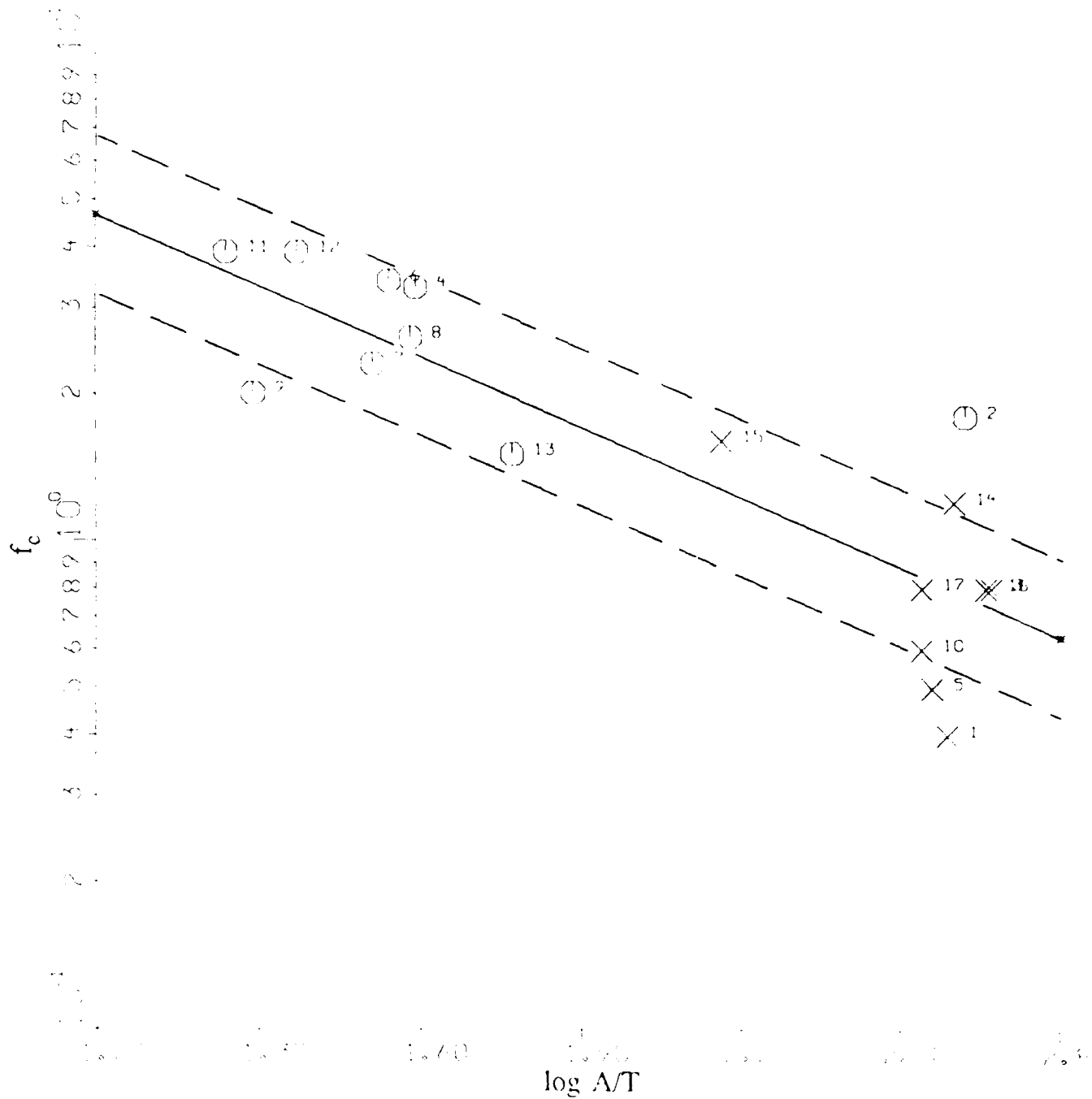
Figure 11a. f_c versus log A/T for 8 below water table (denoted by X) and 9 above water table (marked by circles) shots based on t* = 0.4. The least squares linear regression through all 17 data points (continuous line) has correlation coefficient of 0.851, slope of -0.480, and intercept of 1.148. One SD variation in the intercept value is shown by the dashed lines.

Figure 11b. Similar to Figure 11a for only 8 below water table shots. Forcing a slope of -0.480, the least squares linear regression (continuous line) has intercept of 1.102.
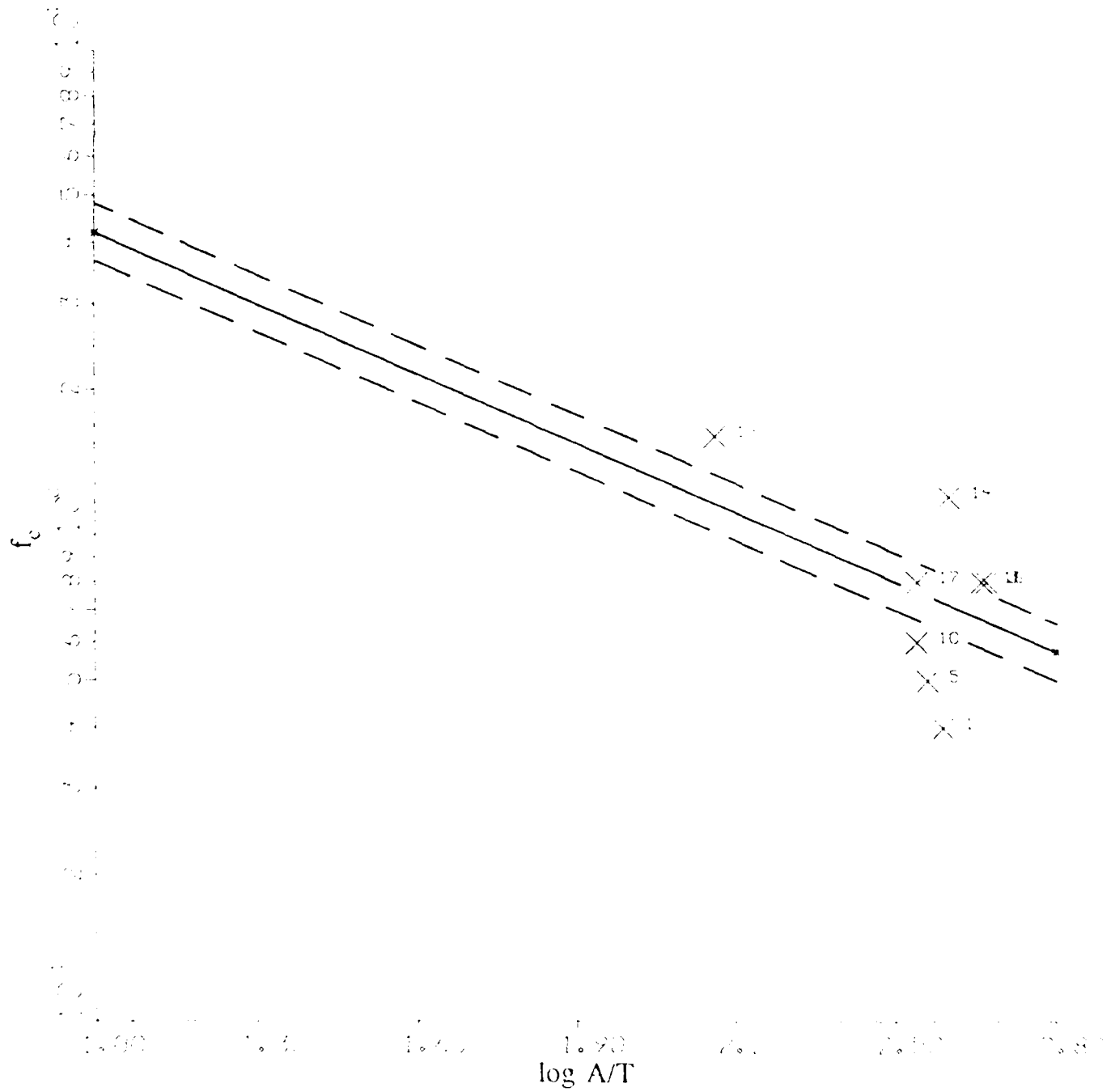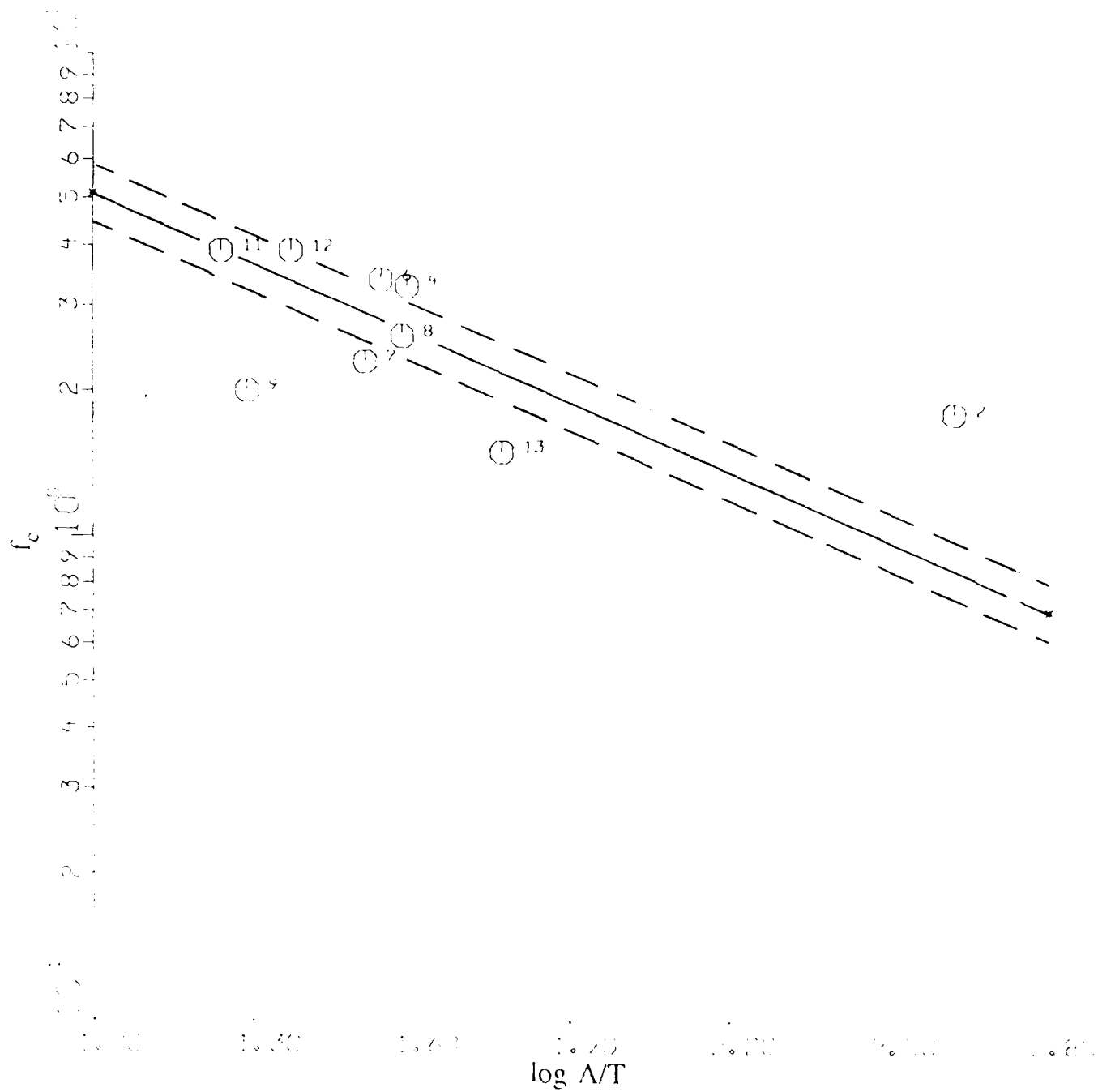
Figure 11c. Similar to Figure 11a for only 9 above water table shots. Forcing a slope of -0.480, the least squares linear regression (continuous line) has intercept of 1.189.

separated by 0.676 (0.128). This is close to the separation observed from 22 shots recorded at JAS.

COMPARISON WITH RESULTS FROM LARGER DATA BASES

Blandford and Klouda (1980) measured regional phases including Pn from a large number of NTS explosions recorded at TFO, at epicentral distances of about 550 km. Their results for magnitudes based on amplitude of Pn (the "b" phase) are used here to compare the magnitude versus yield relationships for below above WT shots. The Rainier Mesa shots are considered to be below WT because of a perched water table at shallow depths in the region. A plot of magnitude versus log yield for all available below WT (35) shots shows a correlation coefficient of 0.918, mean slope of 0.744 (0.056) and mean intercept of 4.477 (0.104). Corresponding results from above WT (112) shots are: correlation coefficient 0.796, mean slope 0.899 (0.065), and mean intercept 3.685 (0.065). These plots indicate a magnitude difference of about 0.46 between below and above WT shots of 150 kt each. Note that this value is fairly close to the separation of 0.36 (0.05) obtained for shots recorded at JAS.

Using amplitude data from the ISC bulletins, P. D. Marshall (written communication) obtained maximum likelihood estimates of the seismic magnitude m_b of a large number of NTS explosions. The methodology used is described in detail in Marshall et al. (1986). Out of a total of 300 events, 287 events were found suitable for studying the effect of the water table. Plots of m_b versus log yield for below WT (114) shots indicate correlation coefficient of 0.971, mean slope of 0.754 (0.018), and mean intercept of 4.096 (0.035). Results from 173 above WT shots are: correlation coefficient 0.872, mean slope 0.899 (0.039), and mean intercept 3.491 (0.054). These plots will indicate a magnitude difference of about 0.29 between below and above WT shots of 150 kt each.

An attempt is now made to estimate the effect of water table when, considering the size of the explosion cavity and the surrounding fracture zone, shots may be considered to be well separated from the water table. A rough measure of the explosion cavity radius R_c is given by

$$R_c = 10 \ Y^{1/3} \tag{8}$$

where Y is the yield in kt. This relationship is not much different from the empirical depth- and medium-dependent relationships for NTS explosion cavity radii obtained by Closmann (1969). One may consider shots having their shot points at least 2 R_c below or above WT to be well separated from the water table. m_b versus log yield plot for 72 well below WT shots (including Rainier Mesa shots which are all assumed to be well below WT) indicated correlation coefficient of 0.981, mean slope of 0.746 (0.017), and mean intercept of 4.118 (0.035). The correlation coefficient for the data from 125 well above WT shots is 0.708, mean slope is 0.711 (0.064), and mean intercept is 3.670 (0.075). These plots indicate the magnitude of a below WT shot to be larger than that of an above WT shot by about 0.52, if each has the same yield of 150 kt. As expected, the separation between the below and above populations is enhanced when only those shots that are well below and well above WT are considered.

EFFECT OF GAS POROSITY AND CAVITY RADII FOR SHOTS IN TUFF

Magnitude versus yield plots for above WT shots show considerably more scatter than those for below WT shots. According to Patton (1988), a possible reason for this is the effect of gas-filled voids in the emplacement medium on source coupling. His investigation based on the use of $m_b(Lg)$ magnitudes showed the gas porosity to significantly reduce m_b (Lg) for shots in tuff (and rhyolite since no distinction was made between the two media, H. J. Patton, oral communication). He also examined the effect of gas porosity on Marshall's m_b values for 21 Yucca shots and found the effect to be very similar to that for m_b (Lg). In this study, we examine a much larger data set consisting of a total of 148 shots (91 below and 57 above WT) from the Yucca Flats, Pahute Mesa, and Rainier Mesa regions of the NTS. These are the only tuff-rhyolite shots for which gas porosity values are available, out of a total of 287 shots for which Marshall's m_b are known.

Approximate expressions for cavity radii in tuff and rhyolite, based on Closmann's (1969) study (see also Mueller and Murphy, 1971), are

$$R_c \text{ (tuff)} = 31.41 \ Y^{0.29} \ h^{-0.11} \tag{9}$$

and

$$R_c \text{ (rhyolite)} = 28.66 \ Y^{0.29} \ h^{-0.11} \tag{10}$$

where h is the shot depth in meters. These two equations were used to determine cavity radii for all 148 tuff-rhyolite shots. Explosions with their shot points at least two cavity radii below the water table and all Rainier Mesa shots may be considered to be well below the water table. There were 56 such shots with known gas porosity and 8 more for which porosity was not known. For these 56 + 8 = 64 well below the water table shots, m_b versus yield rela-

tionship was found to be

$$m_b = 0.744 \ (0.018) \ \log Y + 4.117 \ (0.036). \tag{11}$$

The SD of estimated m_b is 0.109.

A plot of m_b residuals (observed - estimated), where the estimated values are derived for known Y from equation (11), versus gas porosity (in volume %) is shown in Figure 12a for all 148 shots. The usual least squares regression (continuous line), based on the assumption that porosity is error-free, has a mean slope of -0.033 (0.002) and the SD of m_b residual is 0.13. Note that several porosity values in Figure 12a are negative "even though physically unreal as a result of small errors in the measured parameters input to the calculation" (Howard, 1983). Furthermore, there are a large number of shots with exactly zero porosity. All this means that the error in porosity is substantial and should not be neglected. In order to study the effect of errors in both x and y variables, where x denotes porosity and y represents m_b residual, the maximum likelihood linear fitting method of Ericsson (1971) is used to obtain mean slope and intercept values. The variables x and y are assumed to be completely uncorrelated and the ratio $g \equiv \sigma_y/\sigma_x$, where σ denotes the SD, is assumed to be known Since the smallest value of observed porosity for several shots is -5, a rough estimate of σ_x may be assumed to be 5. Similarly, from the data used in equation (11), σ_y is about 0.1 so that g may be taken to be 0.02. The resulting maximum likelihood fit, with derived mean slope value of -0.042 (0.003), is also shown in Figure 12a (dashed line). When 56 well below WT shots are excluded, the results for the remaining 92 shots are shown in Figure 12b. When porosity (x) is assumed to be error-free; the mean slope is -0.034 (0.002) whereas the value increases to -0.043 (0.003) if g = 0.02. If only shots well above WT are considered, the regressions for 31 such shots is shown in Figure 12c. The mean slope changes from -0.026
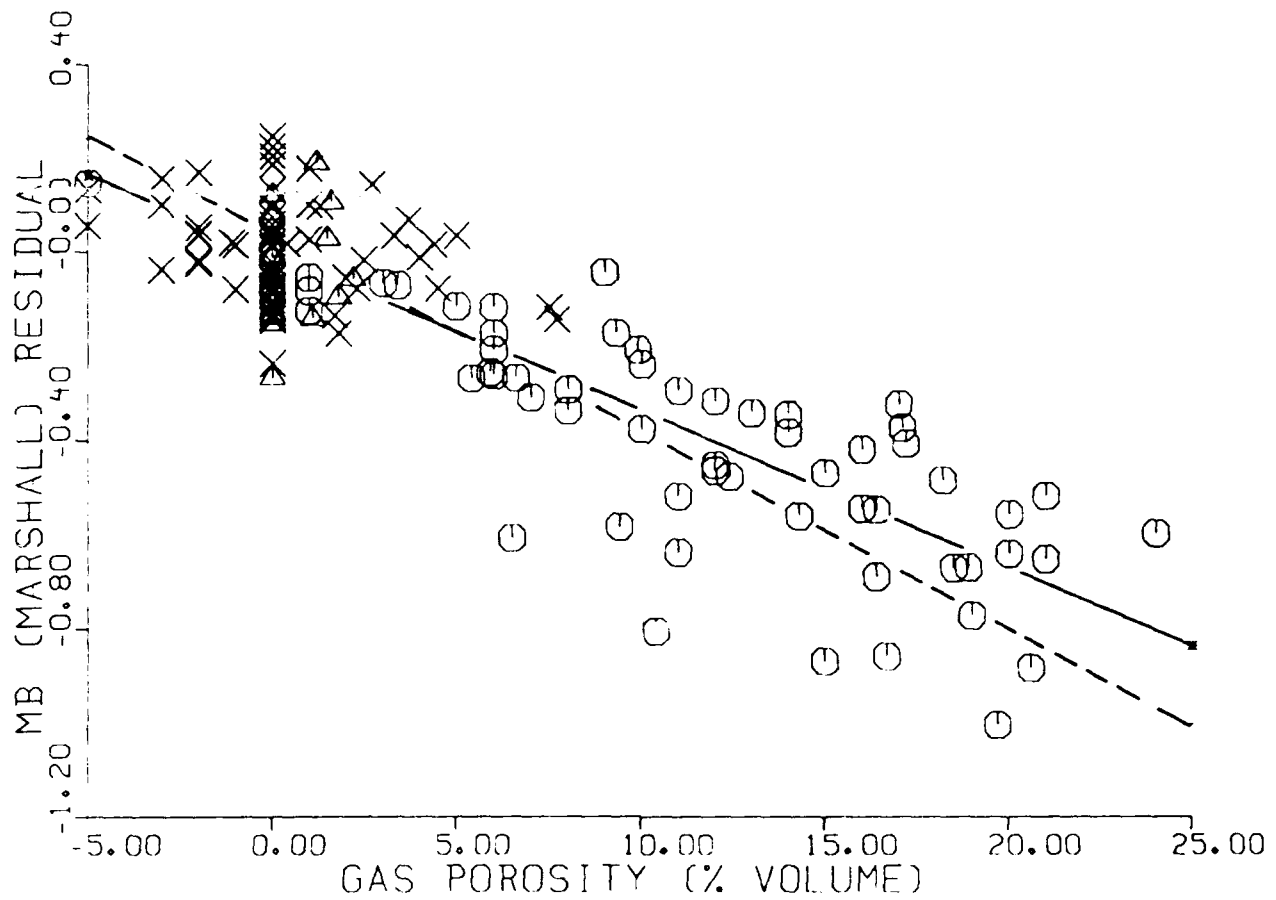
Figure 12a. m_b residual versus gas porosity (in volume %) for 148 tuff-rhyolite shots with known gas porosity values. Below and above water table shots are denoted by X and circle, respectively. The least squares linear regression (continuous line) has a mean slope of -0.033 (0.002) whereas regression based on g = 0.02 (dashed line) shows a larger slope of -0.042 (0.003).
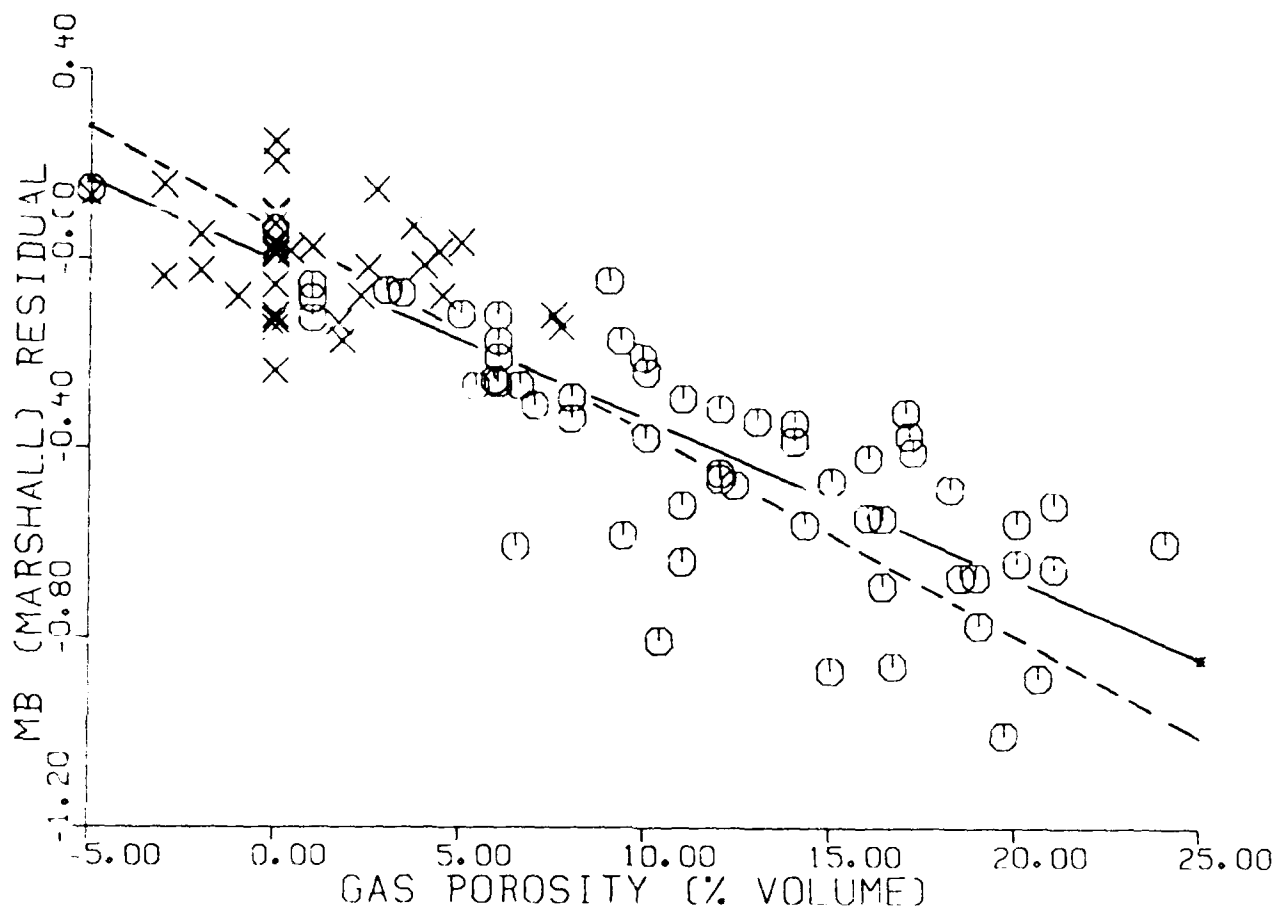
Figure 12b. Similar to Figure 12a for 92 shots obtained by excluding 56 well below water table shots from those used in Figure 12a. The least squares linear regression (continuous line) has a mean slope of -0.034 (0.002) whereas regression based on g = 0.02 (dashed line) shows a larger slope of -0.043 (0.003).
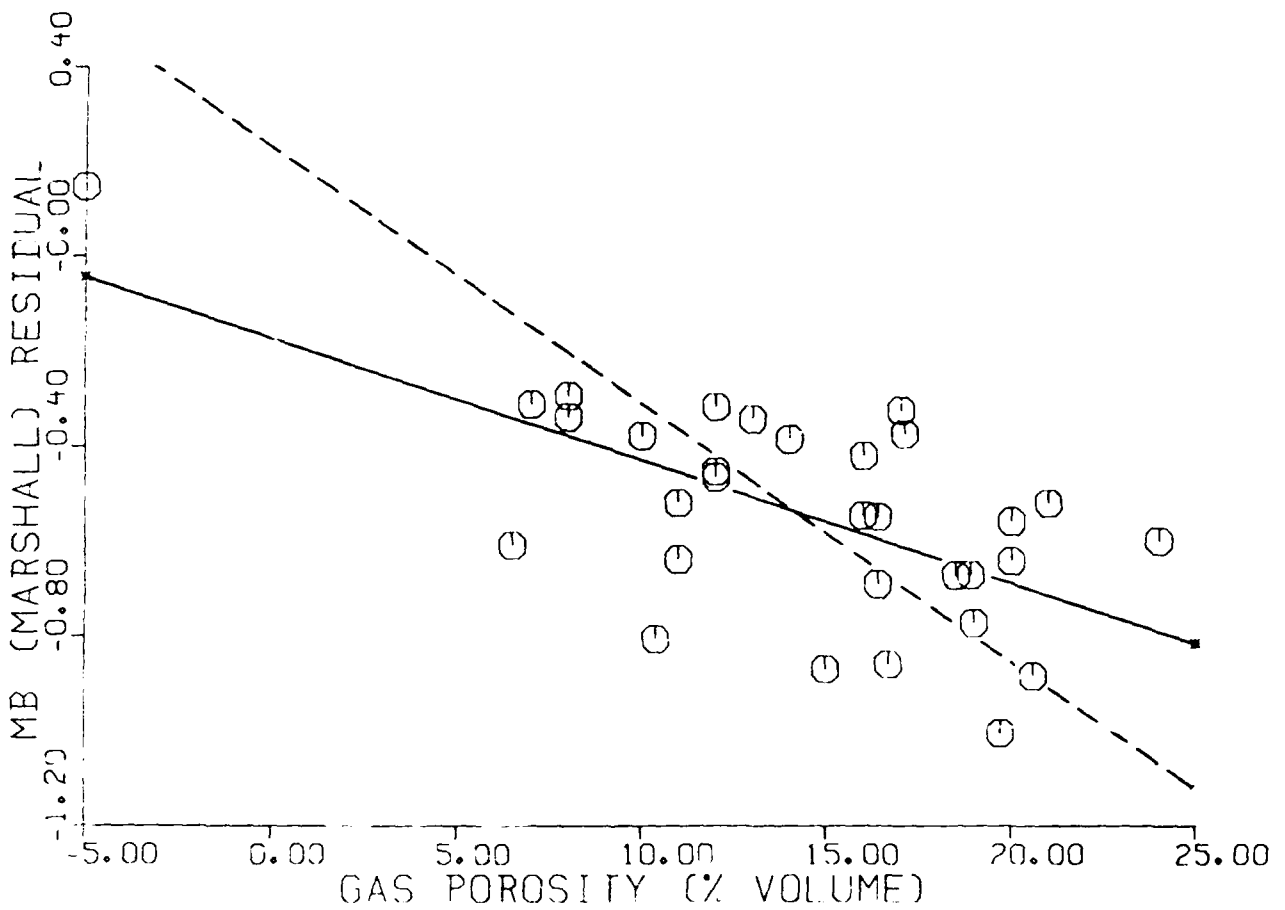
Figure 12c. Similar to Figure 12a for 31 well above water table shots. The least squares linear regression (continuous line) has a mean slope of -0.026 (0.006) whereas regression based on g = 0.02 (dashed line) shows a larger slope of -0.054 (0.016).

(0.006) for error-free x to -0.054 (0.016) for g = 0.02. Note that the mean slopes values based on porosity not being error-free (dashed lines) are all significantly larger than those based on error-free x (continuous lines), thereby suggesting enhanced dependence of m_b residual on gas porosity. All three figures indicate gas porosity to reduce the observed m_b by significant amounts.

We now consider the effect of gas porosity on shots close to the water table, i.e. on $92 - 31 = 61$ shots that are neither well below nor well above WT (i.e. shots within 2 R_c of WT). Plots of m_b residual versus porosity from all 61 shots, a subset of 35 that are below WT, and the remaining 26 above WT shots are shown in Figures 13a, 13b, and 13c, respectively. The mean slopes are -0.029 (0.003), -0.013 (0.007), and -0.027 (0.004) based on error-free x, and -0.039 (0.004), -0.105 (0.025), and -0.036 (0.007) for g – 0.02, respectively. All slope values are negative, confirming the expected effect of gas porosity. Since these 61 shots are all near WT, they should also be expected to show the effect of proximity of their cavity radii and fracture zone to the water table. Defining "scaled distance to water table" (SDWT) as the vertical distance to the water table (considered positive for below and negative for above WT shots, respectively) from the shot point divided by R_c, where R_c is given by equations (9) or (10), the results for 61 (35 below and 26 above WT) shots are shown in Figure 14. Linear regression of the data (continuous line) has a mean slope of 0.141 (0.017), suggesting that explosion cavity and its proximity to the water table significantly influence the source coupling. The lack of a sharp discontinuity where the two populations meet (i.e. at SDWT = 0) means that the distinction between below and above WT shots is lost for shots very close to WT. For explosions with their shot points below WT, shot-generated cavity and surrounding fractures extending above the water table (especially for shots with their cavities
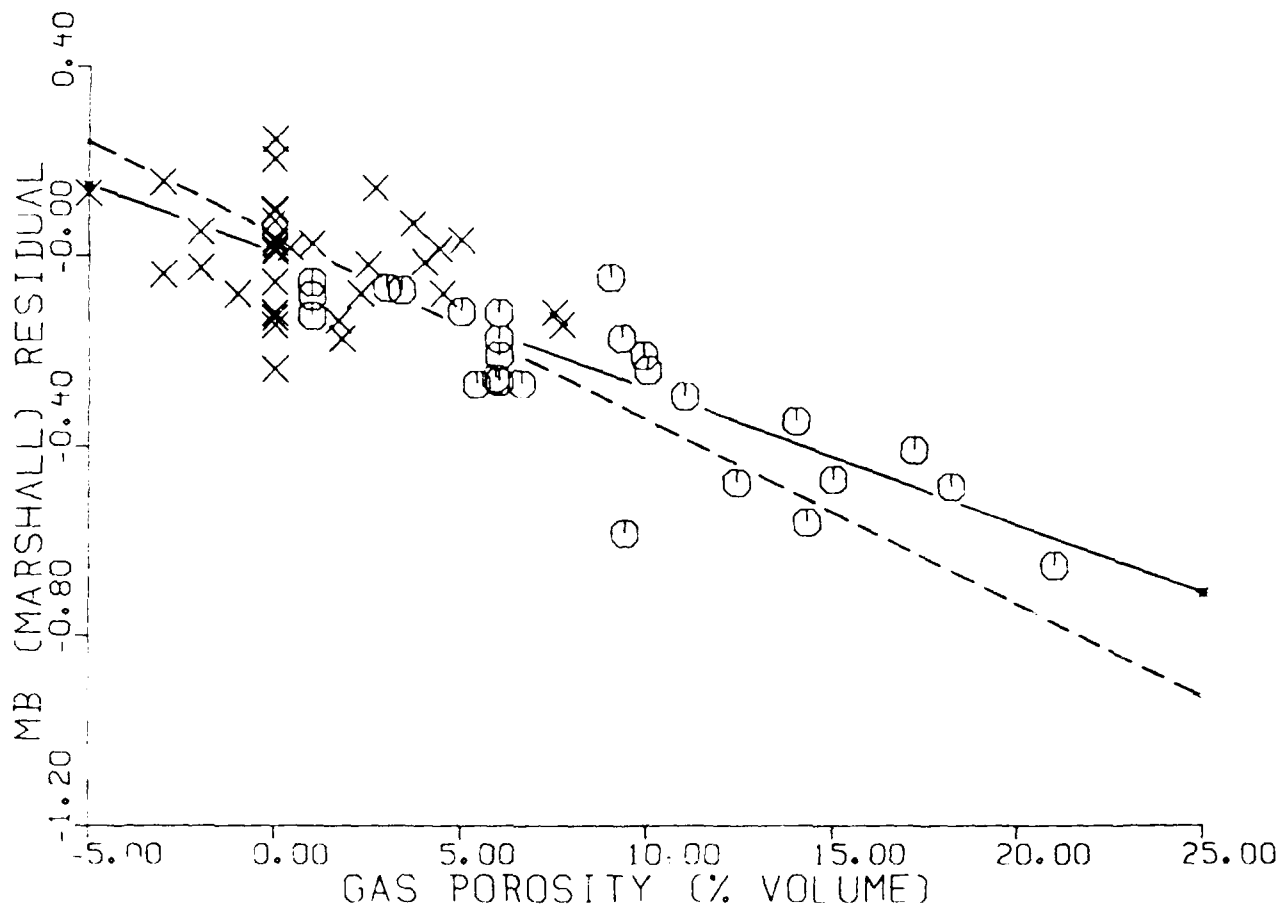
Figure 13a. m_b residual versus gas porosity (in volume %) for 61 tuff-rhyolite shots within 2 cavity radii of the water table. Below and above water table shots are denoted by X and circle, respectively. The least squares linear regression (continuous line) has a mean slope of -0.029 (0.003) whereas regression based on $g = 0.02$ (dashed line) shows a larger slope of -0.039 (0.004).
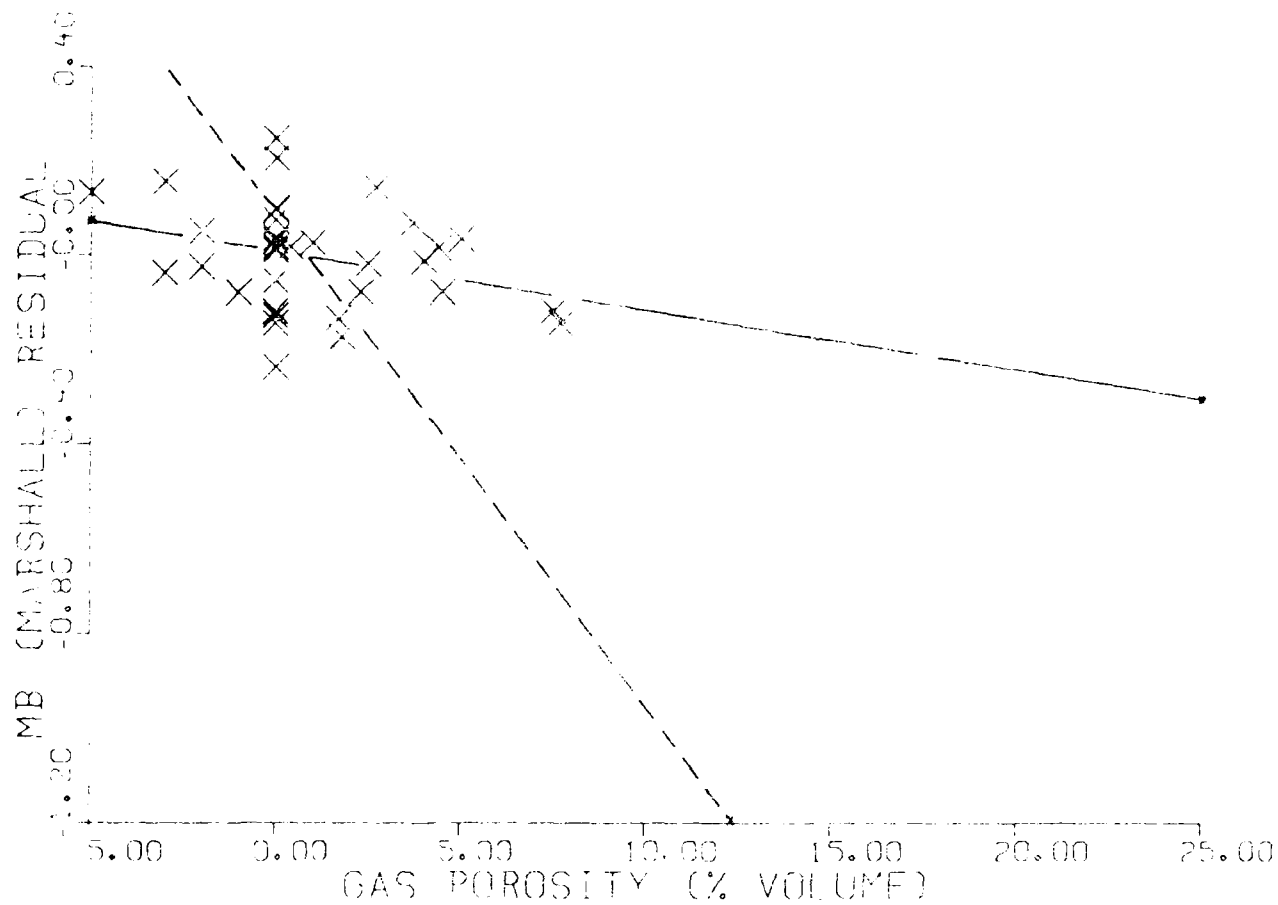
Figure 13b. Similar to Figure 13a for 35 tuff-rhyolite shots that are below but within two cavity radii of the water table. The least squares linear regression (continuous line) has a mean slope of -0.013 (0.007) whereas regression based on g = 0.02 (dashed line) shows a larger slope of -0.105 (0.025).
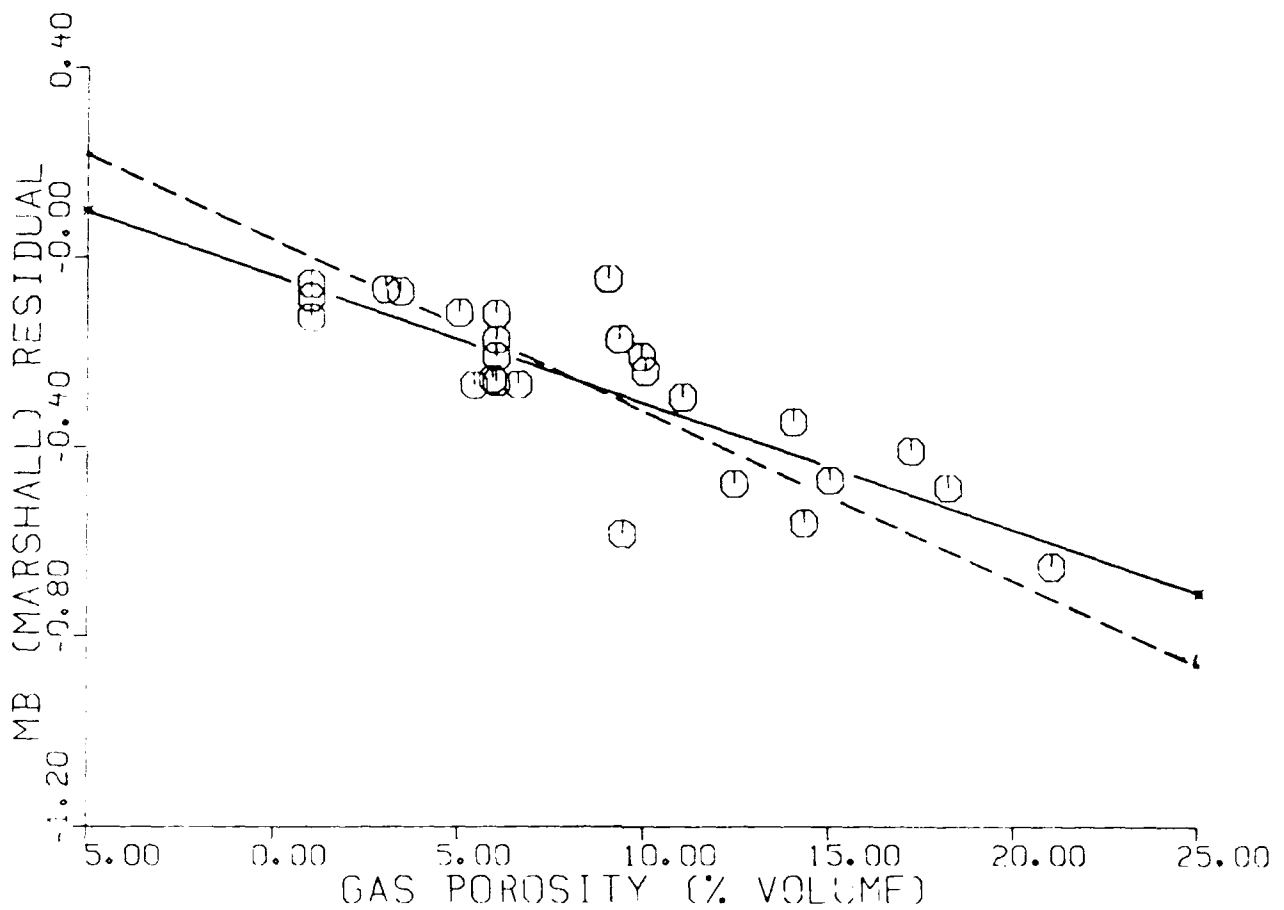
Figure 13c. Similar to Figure 13a for 26 tuff-rhyolite shots that are above but within two cavity radii of the water table. The least squares linear regression (continuous line) has a mean slope of -0.027 (0.004) whereas regression based on g = 0.02 (dashed line) shows a larger slope of -0.036 (0.007).
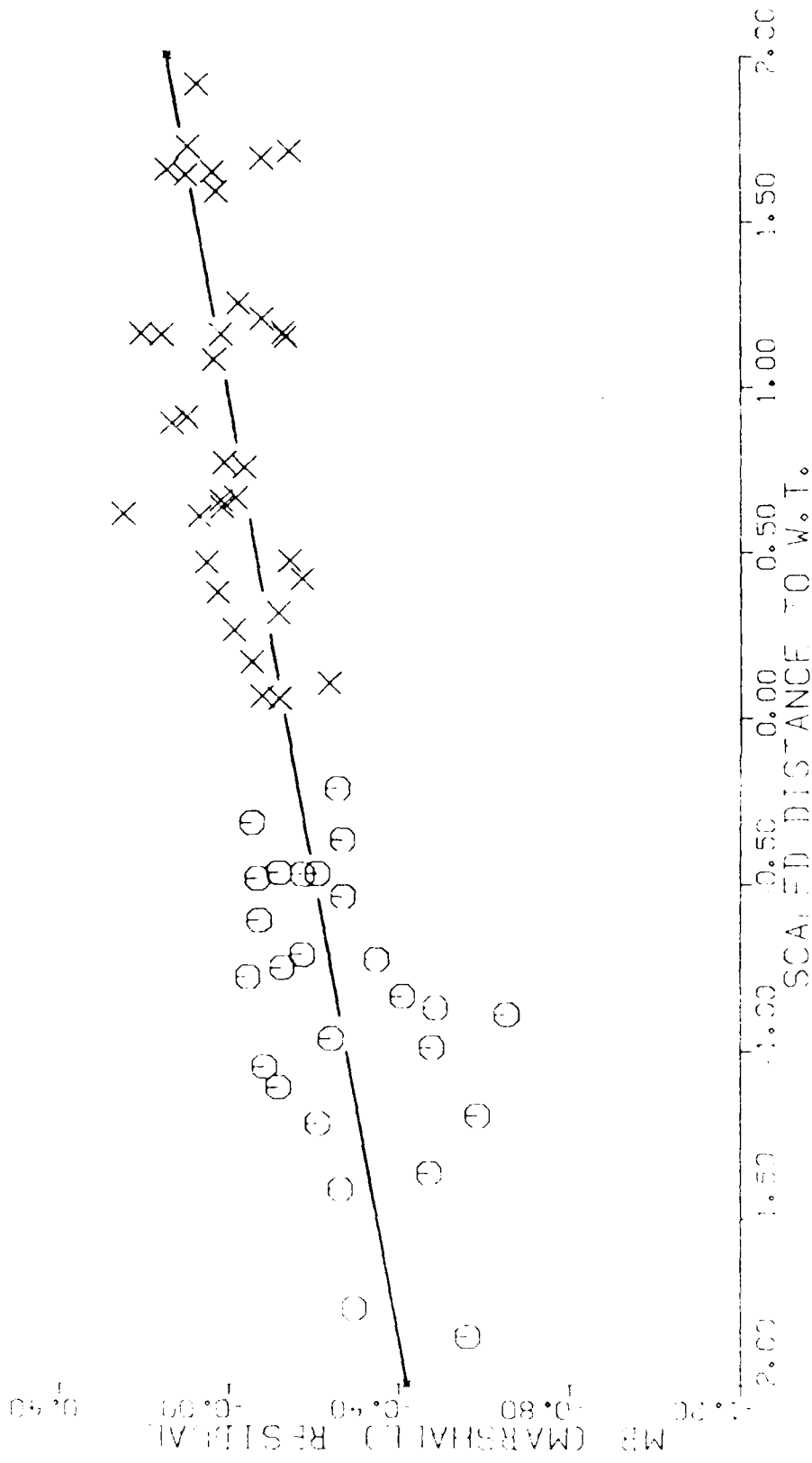
Figure 14. m_b residual versus scaled distance to water table (SDWT) for 61 tuff-rhyolite shots (35 below and 26 above WT, denoted by X and circle, respectively) within two cavity radii of WT. No sharp discontinuity is observed between the below and above WT populations (at SDWT = 0). The least squares regression (continuous line) has a mean slope of 0.141 (0.017) and the SD of m_b residual is 0.135.

49

crossing the water table) appear to reduce the coupling. Similarly, for above WT shots, explosion cavity and fractures intersecting the water table seem to enhance the coupling.

DISCRIMINATION BETWEEN BELOW AND ABOVE WT SHOTS

Analysis of the Pn spectra of 22 shots recorded at JAS shows some separation on plots of f_c versus A_0 derived from the Pn spectra of 22 shots recorded at JAS. However, the separation is probably not large and significant enough to be of much practical value (see Figures 5 and 6). On the other hand, plots of A_0 versus yield show the largest separation between the two types of shots. It seems therefore that the low-frequency spectral amplitude of Pn is a possible discriminant. This is also supported by the spectral ratio of KEARSARGE (above WT shot) to JORNADA (below WT shot) in Figure 3 in which, at low frequencies, the amplitude ratio is much smaller than 1.

The low-frequency amplitude values may also be obtained by bandpassing the data and computing the root-mean-square (RMS) amplitudes, after correcting for the instrumental response and noise level before the onset of direct Pn. Results for the 05-1.5 Hz passband, with window length of 6.4 sec, for the 22 shots recorded at JAS are shown in Figure 15. The least squares regression lines for the two types of shots, assuming a slope of 1, are separated by 0.542 magnitude unit. These results are, as expected, nearly identical with those for A_0. The below WT shots show larger deviations from the mean than the above WT shots. The RMS value from one shot (SALUT) in Figure 15, denoted by the letter P, is close to that expected for an above WT shot. A possible reason for this may be the fact that this is the only below WT shot with non-zero gas porosity value (viz. 4%).

An important factor contributing to the scatter in Figure 15 is perhaps proximity of the shot cavities of several explosions to the water table. Out of a total of 22 shots, the shot points of 3 are within one cavity radius of WT (marked by long arrows) and those of 9 other
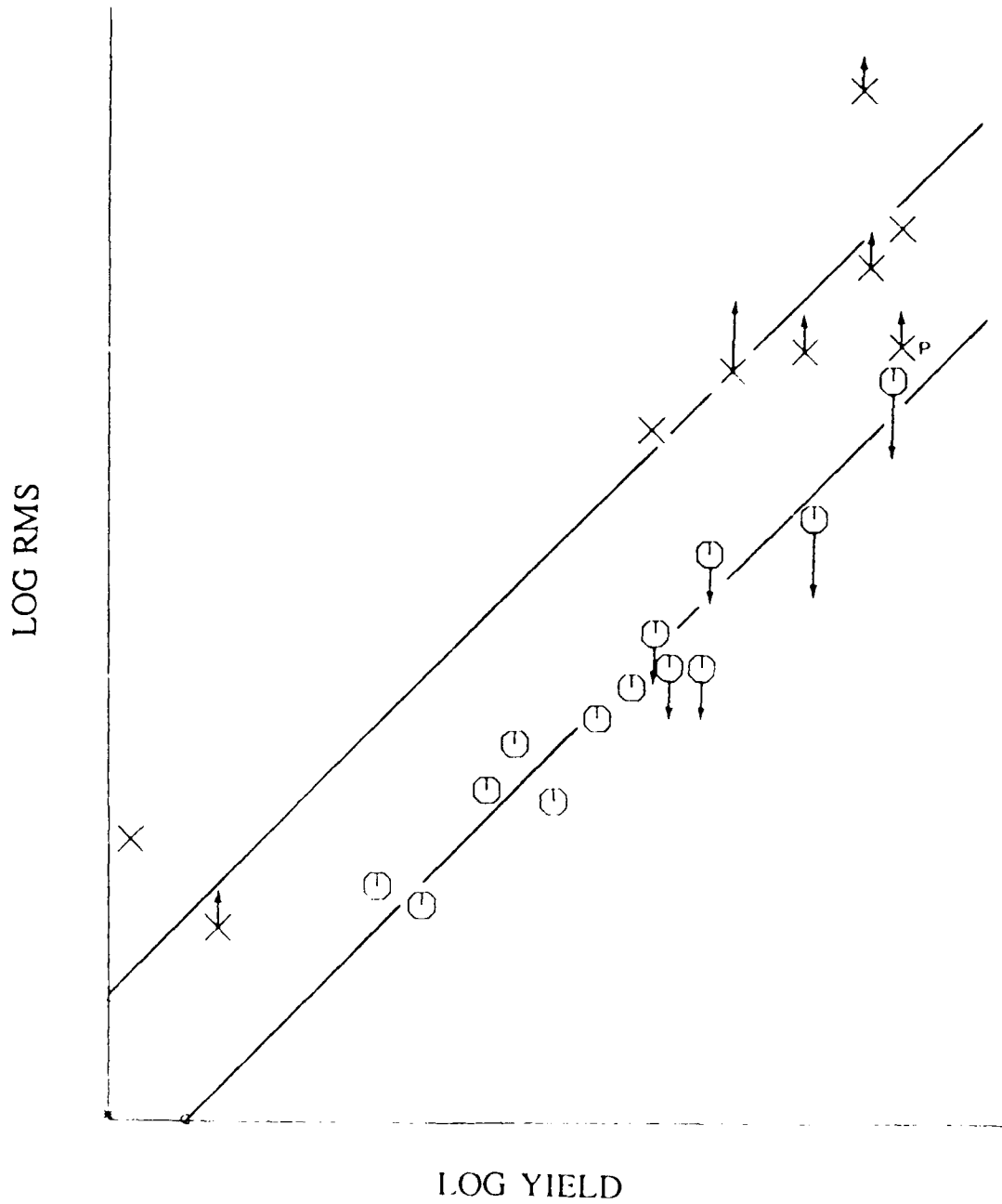
Figure 15. RMS amplitudes of Pn, for the bandpass 0.5 to 1.5 Hz, versus yield for 22 shots recorded at JAS. The mean lines with slope of unity for the below and above WT populations are separated by 0.542 magnitude unit. The arrows indicate explosions with shot points within two cavity radii of the water table.

are within two cavity radii of WT (denoted by small arrows). If this were not the case, the RMS values for these 12 shots would move towards the direction pointed by the arrows, thereby resulting in somewhat larger separation between the two types of shots.

A plot of the RMS values for Lg with window length of 51.2 sec (but otherwise obtained in the same manner as for Pn) versus yield for 19 shots for which Lg was available (most others were clipped) is shown in Figure 16. The below and above WT populations are separated by 0.300 magnitude unit. It seems therefore that Lg is considerably less sensitive than Pn to whether the shot is below or above WT and Pn/Lg amplitude ratio is a possible discriminant. This is in agreement with an analysis of Blandford and Klouda's (1980) data showing larger separation between below and above WT shots for m_b (Pn) than for m_b (Lg).
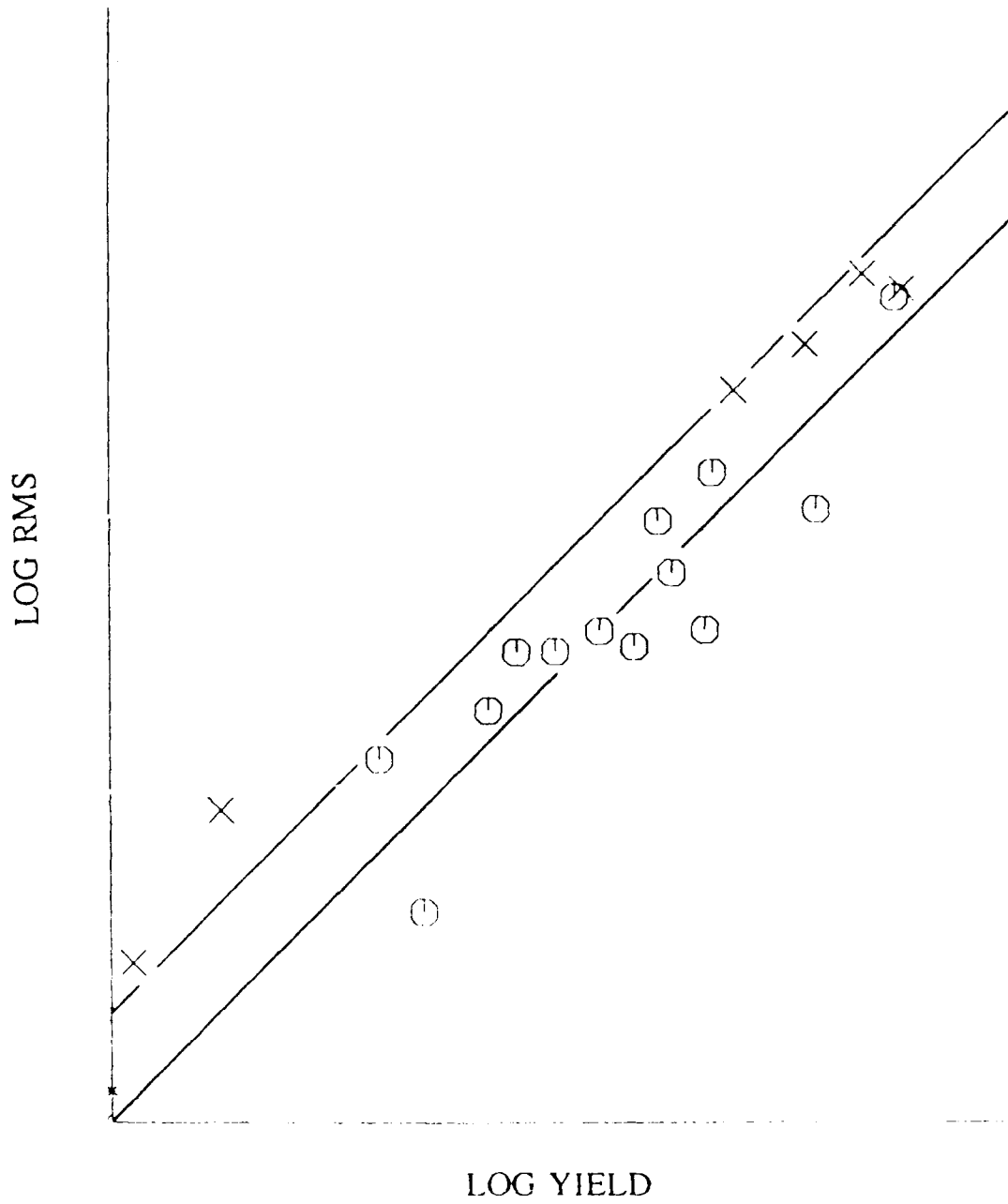
Figure 16. Similar to Figure 15 for Lg. The two mean lines are separated by only 0.300 magnitude unit.

DISCUSSION AND CONCLUSION

Records of JORNADA and KEARSARGE, with good S/N, are also available at the SRO station, ANMO at epicentral distance of about 900 km. The two records are shown in Figure 17. Note that just as in Figure 1, JORNADA has much larger amplitudes than KEARSARGE in the first several seconds of Pn but not so in the later wavetrain. The spectra of Pn (6.4 sec window) for the two shots are shown in Figure 18; S/N is good up to about 6 Hz. The spectral ratio KEARSARGE/JORNADA is shown in Figure 19 and appears similar to that in Figure 3 although the mean slope value is slightly larger. The spectral fits, based on $t^* = 0.25$, are shown in Figure 20 and show differences between the two shots that are similar to those in Figure 4. One may thus conclude that the differences in the spectral characteristics of these two shots, as observed at ANMO, are similar to those observed at JAS and the nearby station CMB.

A comparison of the spectral characteristics of below and above WT shots shows that for most parameters, there is a lack of systematic differences and considerable overlap between the two types of shots, even though records from the same station are used so that source-receiver paths are not much different. This is not surprising in view of the extreme variability of regional phases from NTS explosions at essentially the same location noted by Springer and Denny (1976, especially their Figure 4) and Gupta et al. (1984, see their Figure 11). Plots of f_c versus A_0 appear to show some separation between below and above WT shots recorded at JAS (Figures 5b, c and 6b, c). This separation is, however, not evident in the RSSD data (Figures 10b, c), perhaps because the RSSD results are not as reliable due to poor overlap in the f_c and A_0 values of the below and above WT populations. More data from several other stations should be examined to explore further the possibility of distinguishing between below

(a)

JORNADA (ANMO)--BWT
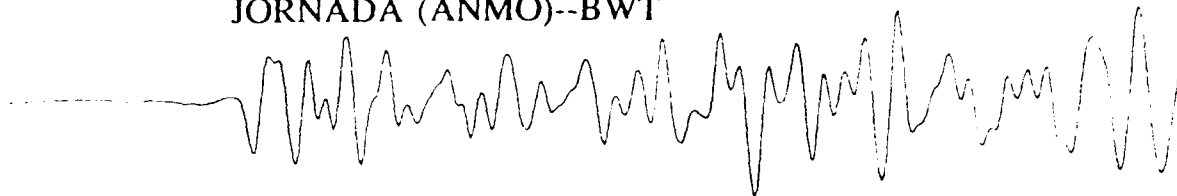
4.0 SEC   105.6 NM 0 P

(b)

KEARSARGE (ANMO)--AWT
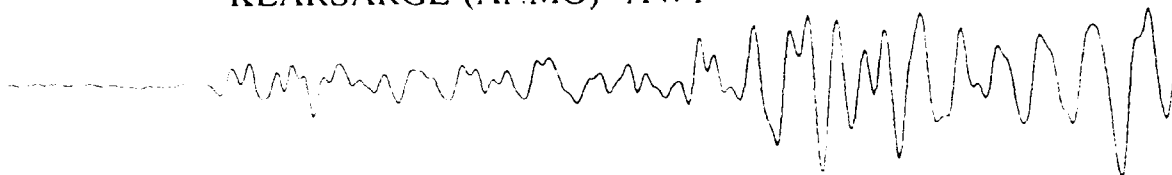
4.0 SEC   105.1 NM 0 P

Figure 17. Short-period, vertical-component records of JORNADA (below water table) and KEARSARGE (above water table) at ANMO, similar to those in Figure 1. Note that in the first several seconds of Pn, KEARSARGE has much smaller amplitude than JORNADA.

Figure 18. Vertical-component displacement amplitude spectra of Pn (6.4 sec long window), similar to those in Figure 2, for JORNADA and KEARSARGE recorded at ANMO. S/N appears good up to about 6 Hz only.

KEARSARGE (ANMO) / JORNADA (ANMO)
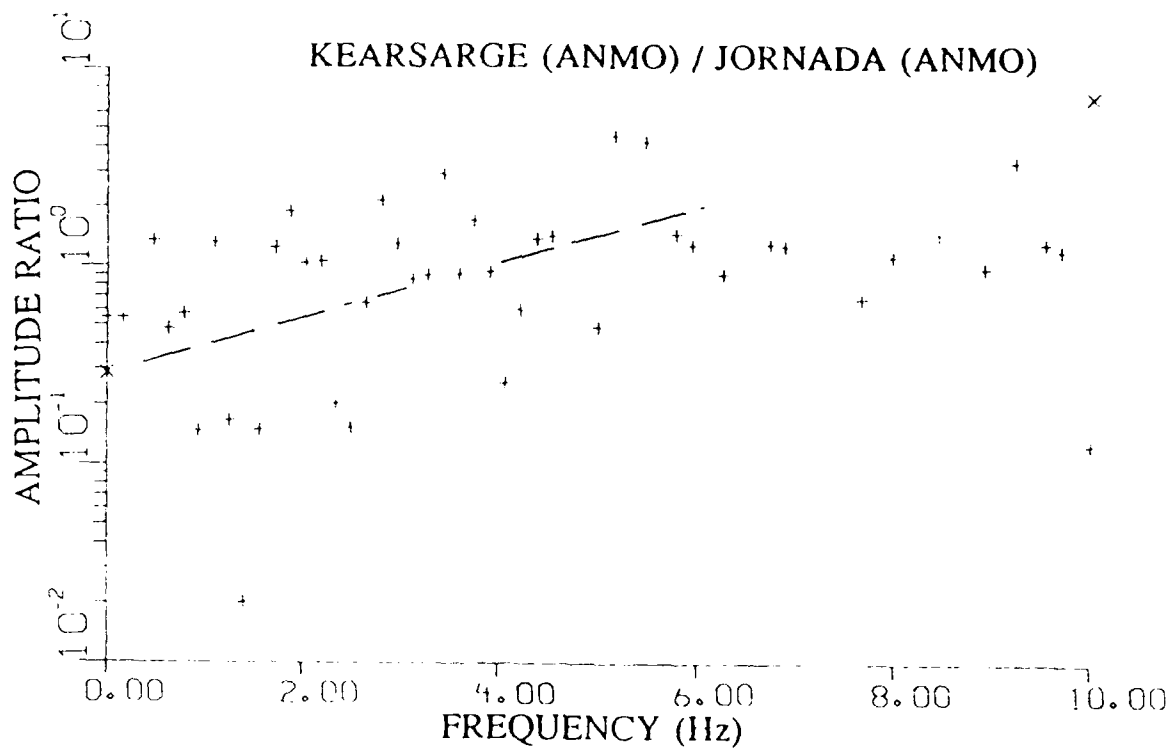
FREQ	BAND	SLOPE	S.D.	AV INTEG
0.2	6.0	0.142	0.005	-0.105
0.2	10.0	0.005	0.002	-0.005

Figure 19. Spectral ratio KEARSARGE/JORNADA of Pn at ANMO, similar to that in Figure 3.

(a)

JORNADA (ANMO)-BWT

$f : 0.2 - 6.0$ Hz
$f_c : 0.2 - 6.0$ Hz
$df = 0.1$ Hz
$N = 33$
$SD = 0.3159$

$f_c = 1.90$ Hz; $A_0 = 89.5$

FREQUENCY (Hz)

AMPLITUDE

(b)

KEARSARGE (ANMO)-AWT

$f : 0.2 - 6.0$ Hz
$f_c : 0.2 - 6.0$ Hz
$df = 0.1$ Hz
$N = 27$
$SD = 0.3026$

$f_c = 5.30$ Hz; $A_0 = 28.4$

FREQUENCY (Hz)

AMPLITUDE

Figure 20. Displacement spectral fits of (a) JORNADA and (b) KEARSARGE at ANMO for corner frequency, f_c, and low-frequency spectral level, A_0, similar to those in Figure 4.

and above WT shots from measurements of their f_c and A_0 values. Broadband instruments are recommended so that both A_0 and f_c are better constrained. A determination fro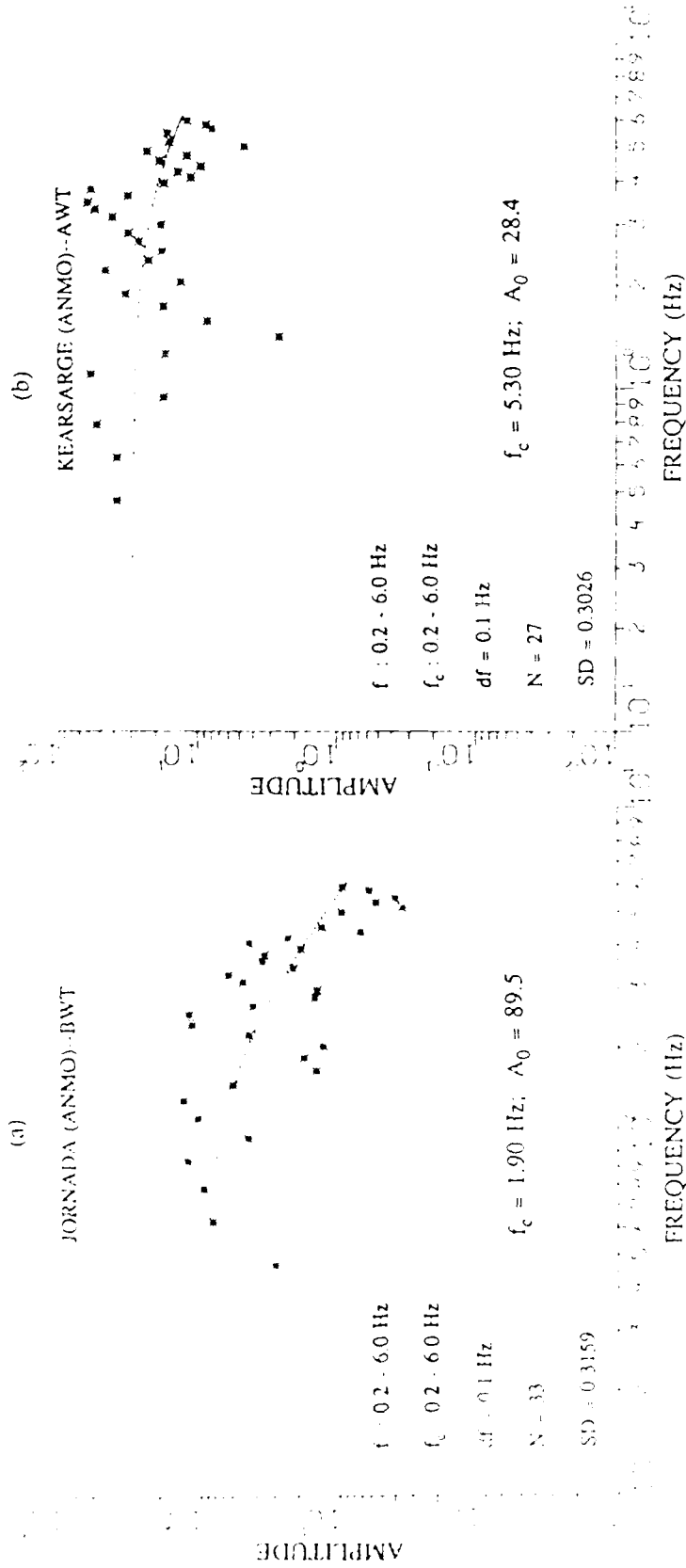m seismic data alone of whether a shot was fired below or above WT is important since it can substantially improve yield estimates. Plots of f_c versus A/T and f_c versus yield show no observable distinction between the two types of shots. The largest systematic difference between below and above WT shots lies in plots of A_0 versus yield and, to a somewhat smaller degree, in plots of A/T (a measure of m_b) versus yield.

Analysis of both regional and teleseismic m_b data from substantially larger data bases also demonstrate that, for a given yield, m_b values for shots below WT are generally larger than those for shots above WT by 0.3 to 0.5 magnitude unit. Gas porosity of the shot medium appears to play an important role in the determination of this large magnitude bias. Yield estimates can be significantly improved if it is known whether the shot point is below or above the water table. A knowledge of the gas-filled porosity of the shot medium may further improve the precision of yield determinations of shots above the water table.

A surprising and interesting result is the important role played by explosion cavity radii in determining the source coupling. The correlation between m_b residual and SDWT (positive for below and negative for above WT shots) for shot points within two cavity radii of WT makes a strong case for the influence of explosion cavity and associated fracture zone on source coupling. Significant improvement in yield estimates can be achieved by combining m_b values with both gas porosity and SDWT where the latter may be computed using empirical medium- and depth-dependent relationships for explosion cavity radii. A comparison of Pn and Lg phases recorded at a common station may be effective in distinguishing below and above WT shots except those that are fired close to the water table.

ACKNOWLEDGMENTS

REFERENCES

Aki, K. and P. G. Richards (1980). *Quantitative Seismology*, W. H. Freeman and Company, San Francisco, California.

Bache, T. C. (1982). Estimating the yield of underground nuclear explosions, *Bull. Seism. Soc. Am. 72*, S131-S168.

Bakun, W. H. and L. R. Johnson (1970). Short period spectral discriminants for explosions, *Geophys. J. R. Astr. Soc. 22*, 139-152.

Blandford, R. R. and P. Klouda (1980). Magnitude-yield results at the Tonto Forest Observatory, in Studies of seismic wave characteristics at regional distances, *AL-80-1*, Teledyne Geotech, Alexandria, Virginia.

Brune, J. N. (1970). Tectonic stress and the spectra of seismic shear waves from earthquakes, *J. Geophys. Res. 75*, 4997-5009; Correction, *J. Geophys. Res. 76*, 5002.

Closmann, P. J. (1969). On the prediction of cavity radius produced by an underground nuclear explosion, *J. Geophys. Res. 74*, 3935-3939.

Ericsson, U. (1971). Maximum likelihood linear fitting when both variables have normal and correlated errors, *FOA 4 Report No. C4474-A1*, Research Institute of National Defense, Stockholm, Sweden.

Evernden, J. F., C. B. Archambeau, and E. Cranswick (1986). An evaluation of seismic decoupling and underground nuclear test monitoring using high-frequency seismic data, *Rev. of Geophysics 24*, 143-215.

Gupta, I. N. and R. R. Blandford (1987). A study of P waves from Nevada Test Site explosions: Near-source information from teleseismic observations? *Bull. Seism. Soc. Am., 77*, 1041-1056.

Gupta, I. N., J. A. Burnetti, R. A. Wagner, and M. Marshall (1984). Discrimination between quarry blasts, nuclear explosions, and earthquakes, *TGAL-TR-84-1*, Teledyne Geotech, Alexandria, Virginia.

Howard, N. W. (1983). Lawrence Livermore National Laboratory, Livermore, California. containment program nuclear test effects and geologic data base: glossary and parameter definitions, *UCID-18300, Part 1, REvision 1*, Lawrence Livermore National Laboratory, Livermore, California.

Marshall, P. D., R. C. Lilwall, and J. Farthing (1986). Body wave magnitudes and locations of underground nuclear explosions at the Nevada Test Site, 1971-1980, *AWRE O 21/86*, H. M. Stationery Office, London.

McLaughlin, K. L., M. E. Marshall, R. A. Wagner, I. N. Gupta, T. W. McElfresh, and A. C. Lees (1987). A study of explosion source functions and amplitudes using available far-field seismic data, *TGAL-87-06*, Teledyne Geotech, Alexandria, Virginia.

Mueller, R. A. and J. R. Murphy (1971). Seismic characteristics of underground nuclear detonations, Part I. Seismic spectrum scaling, *Bull. Seism. Soc. Am. 61*, 1675-1692.

Murphy, J. R. (1981). P wave coupling of underground explosions in various geologic media, in *Identification of Seismic Sources - Earthquake or Underground Explosion*, E. S.

Husebye and S. Mykkeltveit, Editors, D. Reidel Publishing Co., Dordrecht, Holland, 201-205.

Patton, H. J. (1988). Application of Nuttli's method to estimate yield of Nevada Test Site explosions recorded on Lawrence Livermore National Laboratory's digital seismic system, *Bull. Seism. Soc. Am. 78*, 1759-1772.

Shumway, R. H. (1988). *Applied Statistical Time Series Analysis*, Prentice Hall, Englewood Cliffs, New Jersey.

Springer, D. L. (1966). P-wave coupling of underground nuclear explosions, *Bull. Seism. Soc. Am., 56*, 861-876.

Springer, D. L. and M. D. Denny (1976). Seismic spectra of events at regional distances, *UCRL-52048*, Lawrence Livermore National Laboratory, Livermore, California.

Taylor, S. R., N. W. Sherman. and M. D. Denny (1987). Spectral discrimination between NTS explosions and Western U.S. earthquakes at regional distances, *UCRL-97349*. Lawrence Livermore National Laboratory, Livermore, California.

Werth, G. C. and R. F. Herbst (1963). Comparison of amplitudes of seismic waves from nuclear explosions in four mediums, *J. Geophys. Res. 68*, 1463-1475.

Professor Keiiti Aki
Center for Earth Sciences
University of Southern California
University Park
Los Angeles, CA 90089-0741

Professor Thomas Ahrens
Seismological Lab, 252-21
Div. of Geological and Planetary
   Sciences
California Institute of Technology
Pasadena, CA 91125

Professor Charles B. Archambeau
Cooperative Institute for Resch
   in Environmental Sciences
University of Colorado
Boulder, CO 80309

Dr. Thomas C. Bache Jr.
Science Applications Int'l Corp.
10210 Campus Point Drive
San Diego, CA 92121   (2 copies)

Dr. Muawia Barazangi
Institute for the Study of
   of the Continent
Cornell University
Ithaca, NY 14853

Dr. Douglas R. Baumgardt
Signal Analysis & Systems Div.
ENSCO, Inc.
5400 Port Royal Road
Springfield, VA 22151-2388

Dr. Jonathan Berger
Institute of Geophysics and
   Planetary Physics
Scripps Institution of Oceanography
A-025
University of California, San Diego
La Jolla, CA 92093

Dr. S. Bratt
Science Applications Int'l Corp.
10210 Campus Point Drive
San Diego, CA 92121

Dr. Lawrence J. Burdick
Woodward-Clyde Consultants
P.O. Box 93245
Pasadena, CA 91109-3245 (2 copies)

Professor Robert W. Clayton
Seismological Laboratory/Div. of
   Geological & Planetary Sciences
California Institute of Technology
Pasadena, CA 91125

Dr Karl Coyner
New England Research, Inc.
76 Olcott Drive
White River Junction, VT 05001

Dr. Vernon F. Cormier
Department of Geology & Geophysics
U-45, Room 207
The University of Conneticut
Storrs, Connecticut 06268

Dr. Steven Day
Dept. of Geological Sciences
San Diego State U.
San Diego, CA 92182

Dr. Zoltan A. Der
ENSCO, Inc.
5400 Port Royal Road
Springfield, VA 22151-2388

Professor John Ferguson
Center for Lithospheric Studies
The University of Texas at Dallas
P.O. Box 830688
Richardson, TX 75083-0688

Professor Stanley Flatte'
Applied Sciences Building
University of California,
Santa Cruz, CA 95064

Dr. Alexander Florence
SRI International
333 Ravenswood Avenue
Menlo Park, CA 94025-3493

Professor Steven Grand
University of Texas at Austin
Dept of Geological Sciences
Austin, TX 78713-7909

Dr. Henry L. Gray
Associate Dean of Dedman College
Department of Statistical Sciences
Southern Methodist University
Dallas, TX 75275

Professor Roy Greenfield
Geosciences Department
403 Deike Building
The Pennsylvania State University
University Park, PA 16802

Professor David G. Harkrider
Seismological Laboratory
Div of Geological & Planetary Sciences
California Institute of Technology
Pasadena, CA 91125

Professor Donald V. Helmberger
Seismological Laboratory
Div of Geological & Planetary Sciences
California Institute of Technology
Pasadena, CA 91125

Professor Eugene Herrin
Institute for the Study of Earth
  and Man/Geophysical Laboratory
Southern Methodist University
Dallas, TX 75275

Professor Robert B. Herrmann
Department of Earth & Atmospheric
     Sciences
Saint Louis University
Saint Louis, MO 63156

Professor Bryan Isacks
Cornell University
Dept of Geological Sciences
SNEE Hall
Ithaca, NY 14850

Professor Lane R. Johnson
Seismographic Station
University of California
Berkeley, CA 94720

Professor Thomas H. Jordan
Department of Earth, Atmospheric
 and Planetary Sciences
Mass Institute of Technology
Cambridge, MA 02139

Dr. Alan Kafka
Department of Geology &
  Geophysics
Boston College
Chestnut Hill, MA 02167

Professor Leon Knopoff
University of California
 Institute of Geophysics
 & Planetary Physics
Los Angeles, CA 90024

Professor Charles A. Langston
Geosciences Department
403 Deike Building
The Pennsylvania State University
University Park, PA 16802

Professor Thorne Lay
Department of Geological Sciences
1006 C.C. Little Building
University of Michigan
Ann Arbor, MI 48109-1063

Dr. Randolph Martin III
New England Research, Inc.
76 Olcott Drive
White River Junction, VT 05001

Dr. Gary McCartor
Mission Research Corp.
735 State Street
P.O. Drawer 719
Santa Barbara, CA 93102   (2 copies)

Professor Thomas V. McEvilly
Seismographic Station
University of California
Berkeley, CA 94720

Dr. Keith L. McLaughlin
S-CUBED,
A Division of Maxwell Laboratory
P.O. Box 1620
La Jolla, CA 92038-1620

Professor William Menke
Lamont-Doherty Geological Observatory
  of Columbia University
Palisades, NY 10964

Professor Brian J. Mitchell
Department of Earth & Atmospheric
  Sciences
Saint Louis University
Saint Louis, MO 63156

Mr. Jack Murphy
S-CUBED
A Division of Maxwell Laboratory
11800 Sunrise Valley Drive
Suite 1212
Reston, VA 22091 (2 copies)

Professor J. A. Orcutt
IGPP, A-205
Scripps Institute of Oceanography
Univ. of California, San Diego
La Jolla, CA 92093

Professor Keith Priestley
University of Nevada
Mackay School of Mines
Reno, NV 89557

Professor Paul G. Richards
Lamont-Doherty Geological
Observatory of Columbia Univ.
Palisades, NY 10964

Wilmer Rivers
Teledyne Geotech
314 Montgomery Street
Alexandria, VA 22314

Dr. Alan S. Ryall, Jr.
Center of Seismic Studies
1300 North 17th Street
Suite 1450
Arlington, VA 22209-2308   (4 copies)

Professor Charles G. Sammis
Center for Earth Sciences
University of Southern California
University Park
Los Angeles, CA 90089-0741

Professor Christopher H. Scholz
Geological Sciences
Lamont-Doherty Geological Observatory
Palisades, NY 10964

Dr. Jeffrey L. Stevens
S-CUBED,
A Division of Maxwell Laboratory
P.O. Box 1620
La Jolla, CA 92038-1620

Professor Brian Stump
Institute for the Study of Earth & Man
Geophysical Laboratory
Southern Methodist University
Dallas, TX 75275

Professor Ta-liang Teng
Center for Earth Sciences
University of Southern California
University Park
Los Angeles, CA 90089-0741

Dr. Clifford Thurber
State University of New York at
   Stony Brooks
Dept of Earth and Space Sciences
Stony Brook, NY 11794-2100

Professor M. Nafi Toksoz
Earth Resources Lab
Dept of Earth, Atmospheric and
   Planetary Sciences
Massachusetts Institute of   Technology
42 Carleton Street
Cambridge, MA 02142

Professor Terry C. Wallace
Department of Geosciences
Building #77
University of Arizona
Tucson, AZ 85721

Weidlinger Associates
ATTN: Dr. Gregory Wojcik
4410 El Camino Real, Suite 110
Los Altos, CA 94022

Professor Francis T. Wu
Department of Geological Sciences
State University of New York
   at Binghamton
Vestal, NY 13901

Dr. Indra N. Gupta
Teledyne Geotech
314 Montgomery St.
Alexandria, VA 22314

Dr. Monem Abdel-Gawad
Rockwell Internat'l Science Center
1049 Camino Dos Rios
Thousand Oaks, CA 91360

Professor Shelton S. Alexander
Geosciences Department
403 Deike Building
The Pennsylvania State University
University Park, PA 16802

Dr. Ralph Archuleta
Department of Geological
   Sciences
Univ. of California at
   Santa Barbara
Santa Barbara, CA

J. Barker
Department of Geological Sciences
State University of New York
 at Binghamton
Vestal, NY   13901

Mr. William J. Best
907 Westwood Drive
Vienna, VA   22180

Dr. N. Biswas
Geophysical Institute
University of Alaska
Fairbanks, AK 99701

Dr. G. A. Bollinger
Department of Geological Sciences
Virginia Polytechnical Institute
21044 Derring Hall
Blacksburg, VA   24061

Mr. Roy Burger
1221 Serry Rd.
Schenectady, NY   12309

Dr. Robert Burridge
Schlumberger-Doll Resch Ctr.
Old Quarry Road
Ridgefield, CT   06877

Science Horizons, Inc.
ATTN: Dr. Theodore Cherry
710 Encinitas Blvd., Suite 101
Encinitas, CA   92024   (2 copies)

Professor Jon F. Claerbout
Professor Amos Nur
Dept. of Geophysics
Stanford University
Stanford, CA   94305 (2 copies)
Dr. Anton W. Dainty
Earth Resources Lab
Massachusetts Institute of Technology
42 Carleton Street
Cambridge, MA   02142
Professor Adam Dziewonski
Hoffman Laboratory
Harvard University
20 Oxford St.
Cambridge, MA   02138

Professor John Ebel
Dept of Geology and Geophysics
Boston College
Chestnut Hill, MA   02167

Dr. Donald Forsyth
Dept of Geological Sciences
Brown University
Providence, RI   02912

Dr. Anthony Gangi
Texas A&M University
Department of Geophysics
College Station, TX   77843

Dr. Freeman Gilbert
Institute of Geophysics &
   Planetary Physics
University of California, San Diego
P.O. Box 109
La Jolla, CA   92037

Mr. Edward Giller
Pacific Seirra Research Corp.
1401 Wilson Boulevard
Arlington, VA   22209

Dr. Jeffrey W. Given
Sierra Geophysics
11255 Kirkland Way
Kirkland, WA 98033

Rong Song Jih
Teledyne Geotech
314 Montgomery Street
Alexandria, Virginia 22314

Professor F.K. Lamb
University of Illinois at
  Urbana-Champaign
Department of Physics
1110 West Green Street
Urbana, IL 61801

Dr. Arthur Lerner-Lam
Lamont-Doherty Geological Observatory
 of Columbia University
Palisades, NY 10964

Dr. L. Timothy Long
School of Geophysical Sciences
Georgia Institute of Technology
Atlanta, GA 30332

Dr. Peter Malin
University of California at
  Santa Barbara
Institute for Central Studies
Santa Barbara, CA 95106

Dr. George R. Mellman
Sierra Geophysics
11255 Kirkland Way
Kirkland, WA 98033

Dr. Bernard Minster
IGPP, A-205
Scripps Institute of Oceanography
Univ. of California, San Diego
La Jolla, CA 92093

Professor John Nabelek
College of Oceanography
Oregon State University
Corvallis, OR 97331

Dr. Geza Nagy
U. California, San Diego
Dept of Ames, M.S. B-010
La Jolla, CA 92093

Dr. Jack Oliver
Department of Geology
Cornell University
Ithaca, NY 14850

Dr. Robert Phinney/Dr. F. A. Dahlen
Dept of Geological
Geological Science University
Princeton University
Princeton, NJ 08540

RADIX System, Inc.
Attn: Dr. Jay Pulli
2 Taft Court, Suite 203
Rockville, Maryland 20850

Dr. Norton Rimer
S-CUBED
A Division of Maxwell Laboratory
P.O. 1620
La Jolla, CA 92038-1620

Professor Larry J. Ruff
Department of Geological Sciences
1006 C.C. Little Building
University of Michigan
Ann Arbor, MI 48109-1063

Dr. Richard Sailor
TASC Inc.
55 Walkers Brook Drive
Reading, MA 01867

Thomas J. Sereno, Jr.
Science Application Int'l Corp.
10210 Campus Point Drive
San Diego, CA 92121

Dr. David G. Simpson
Lamont-Doherty Geological Observ.
 of Columbia University
Palisades, NY 10964

Dr. Bob Smith
Department of Geophysics
University of Utah
1400 East 2nd South
Salt Lake City, UT 84112

Dr. S. W. Smith
Geophysics Program
University of Washington
Seattle, WA 98195

Dr. Stewart Smith
IRIS Inc.
1616 N. Fort Myer Drive
Suite 1440
Arlington, VA 22209

Rondout Associates
ATTN: Dr. George Sutton,
Dr. Jerry Carter, Dr. Paul Pomeroy
P.O. Box 224
Stone Ridge, NY 12484   (4 copies)

Dr. L. Sykes
Lamont Doherty Geological Observ.
Columbia University
Palisades, NY 10964

Dr. Pradeep Talwani
Department of Geological Sciences
University of South Carolina
Columbia, SC 29208

Dr. R. B. Tittmann
Rockwell International Science Center
1049 Camino Dos Rios
P.O. Box 1085
Thousand Oaks, CA 91360

Professor John H. Woodhouse
Hoffman Laboratory
Harvard University
20 Oxford St.
Cambridge, MA 02138

Dr. Gregory B. Young
ENSCO, Inc.
5400 Port Royal Road
Springfield, VA 22151-2388

Dr. Gregory van der Vink
IRIS
Suite 1440
1616 North Fort Myer Drive
Arlington, VA 22209

Dr. Peter Basham
Earth Physics Branch
Geological Survey of Canada
1 Observatory Crescent
Ottawa, Ontario
CANADA K1A 0Y3

Professor Ari Ben-Menahem
Dept of Applied Mathematics
Weizman Institute of Science
Rehovot
ISRAEL 951729

Dr. Eduard Berg
Institute of Geophysics
University of Hawaii
Honolulu, HI 96822

Dr. Michel Bouchon - Universite
   Scientifique et Medicale de Grenob
Lab de Geophysique - Interne et
   Tectonophysique - I.R.I.G.M-B.P.
38402 St. Martin D'Heres
Cedex FRANCE

Dr. Hilmar Bungum/NTNF/NORSAR
P.O. Box 51
Norwegian Council of Science,
Industry and Research, NORSAR
N-2007 Kjeller, NORWAY

Dr. Michel Campillo
I.R.I.G.M.-B.P. 68
38402 St. Martin D'Heres
Cedex, FRANCE

Dr. Kin-Yip Chun
Geophysics Division
Physics Department
University of Toronto
Ontario, CANADA M5S 1A7

Dr. Alan Douglas
Ministry of Defense
Blacknest, Brimpton,
 Reading RG7-4RS
UNITED KINGDOM

Dr. Manfred Henger
Fed. Inst. For Geosciences & Nat'l Res.
Postfach 510153
D-3000 Hannover 51
FEDERAL REPUBLIC OF GERMANY

Ms. Eva Johannisson
Senior Research Officer
National Defense Research Inst.
P.O. Box 27322
S-102 54 Stockholm
SWEDEN

Tormod Kvaerna
NTNF/NORSAR
P.O. Box 51
N-2007 Kjeller, NORWAY

Mr. Peter Marshall, Procurement
 Executive, Ministry of Defense
Blacknest, Brimpton,
 Reading FG7-4RS
UNITED KINGDOM (3 copies)

Dr. Robert North
Geophysics Division
Geological Survey of Canada
1 Observatory crescent
Ottawa, Ontario
CANADA, K1A 0Y3

Dr. Frode Ringdal
NTNF/NORSAR
P.O. Box 51
N-2007 Kjeller, NORWAY

Dr. Jorg Schlittenhardt
Federal Inst. for Geosciences & Nat'l Res.
Postfach 510153
D-3000 Hannover 51
FEDERAL REPUBLIC OF GERMANY

University of Hawaii
Institute of Geophysics
ATTN: Dr. Daniel Walker
Honolulu, HI 96822

Dr. Ramon Cabre, S.J.
Observatorio San Calixto
Casilla 5939
La Paz Bolivia

Professor Peter Harjes
Institute for Geophysik
Rhur University/Bochum
P.O. Box 102148, 4630 Bochum 1
FEDERAL REPUBLIC OF GERMANY

Dr. E. Husebye
NTNF/NORSAR
P.O. Box 51
N-2007 Kjeller, NORWAY

Professor Brian L.N. Kennett
Research School of Earth Sciences
Institute of Advanced Studies
G.P.O. Box 4
Canberra 2601
AUSTRALIA

Dr. B. Massinon
Societe Radiomana
27, Rue Claude Bernard
7,005, Paris, FRANCE   (2 copies)

Dr. Pierre Mechler
Societe Radiomana
27, Rue Claude Bernard
75005, Paris, FRANCE

Dr. Svein Mykkeltveit
NTNF/NORSAR
P.O. Box 51
N-2007 Kjeller, NORWAY   (3 copies)

Dr. Ralph Alewine III
DARPA/NMRO
1400 Wilson Boulevard
Arlington, VA 22209-2308

Dr. Robert Blandford
DARPA/NMRO
1400 Wilson Boulevard
Arlington, VA 22209-2308

Sandia National Laboratory
ATTN: Dr. H. B. Durham
Albuquerque, NM 87185

Dr. Jack Evernden
USGS-Earthquake Studies
345 Middlefield Road
Menlo Park, CA 94025

U.S. Geological Survey
ATTN: Dr. T. Hanks
Nat'l Earthquake Resch Center
345 Middlefield Road
Menlo Park, CA 94025

Dr. James Hannon
Lawrence Livermore Nat'l Lab.
P.O. Box 808
Livermore, CA 94550

Paul Johnson
ESS-4, Mail Stop J979
Los Alamos National Laboratory
Los Alamos, NM 87545

Ms. Ann Kerr
DARPA/NMRO
1400 Wilson Boulevard
Arlington, VA 22209-2308

Dr. Max Koontz
US Dept of Energy/DP 5
Forrestal Building
1000 Independence Ave.
Washington, D.C. 20585

Dr. W. H. K. Lee
USGS
Office of Earthquakes, Volcanoes,
  & Engineering
Branch of Seismology
345 Middlefield Rd
Menlo Park, CA 94025

Dr. William Leith
U.S. Geological Survey
Mail Stop 928
Reston, VA 22092

Dr. Richard Lewis
Dir. Earthquake Engineering and
  Geophysics
U.S. Army Corps of Engineers
Box 631
Vicksburg, MS 39180

Dr. Robert Masse'
Box 25046, Mail Stop 967
Denver Federal Center
Denver, Colorado 80225

Richard Morrow
ACDA/VI
Room 5741
320 21st Street N.W.
Washington, D.C. 20451

Dr. Keith K. Nakanishi
Lawrence Livermore National Laboratory
P.O. Box 808, L-205
Livermore, CA 94550 (2 copies)

Dr. Carl Newton
Los Alamos National Lab.
P.O. Box 1663
Mail Stop C335, Group ESS-3
Los Alamos, NM 87545

Dr. Kenneth H. Olsen
Los Alamos Scientific Lab.
P.O. Box 1663
Mail Stop C335, Group ESS-3
Los Alamos, NM 87545

Howard J. Patton
Lawrence Livermore National
  Laboratory
P.O. Box 808, L-205
Livermore, CA 94550

Mr. Chris Paine
Office of Senator Kennedy
SR 315
United States Senate
Washington, D.C.   20510

AFOSR/NP
ATTN: Colonel Jerry J. Perrizo
Bldg 410
Bolling AFB, Wash D.C.   20332-6448

HQ AFTAC/TT
Attn: Dr. Frank F. Pilotte
Patrick AFB, Florida 32925-6001

Mr. Jack Rachlin
USGS - Geology, Rm 3 C136
Mail Stop 928 National Center
Reston, VA   22092

Robert Reinke
AFWL/NTESG
Kirtland AFB, NM   87117-6008

Dr. Byron Ristvet
HQ DNA, Nevada Operations Office
Attn: NVCG
P.O. Box 98539
Las Vegas, NV   89193

HQ AFTAC/TGR
Attn: Dr. George H. Rothe
Patrick AFB, Florida   32925-6001

Donald L. Springer
Lawrence Livermore National Laboratory
P.O. Box 808, L-205
Livermore, CA   94550

Dr. Lawrence Turnbull
OSWR/NED
Central Intelligence Agency
CIA, Room 5G48
Washington, D.C.   20505

Dr. Thomas Weaver
Los Alamos National Laboratory
P.O. Box 1663
MS C 335
Los Alamos, NM   87545

GL/SULL
Research Library
Hanscom AFB, MA   01731-5000 (2 copies)

Secretary of the Air Force (SAFRD)
Washington, DC   20330
Office of the Secretary Defense
DDR & E
Washington, DC   20330

HQ DNA
ATTN: Technical Library
Washington, DC 20305

DARPA/RMO/RETRIEVAL
1400 Wilson Blvd.
Arlington, VA   22209

DARPA/RMO/Security Office
1400 Wilson Blvd.
Arlington, VA   22209

GL/XO
Hanscom AFB, MA   01731-5000

GL/LW
Hanscom AFB, MA 01731-5000

DARPA/PM
1400 Wilson Boulevard
Arlington, VA 22209

Defense Technical
 Information Center
Cameron Station
Alexandria, VA 22314
(5 copies)

Defense Intelligence Agency
Directorate for Scientific &
 Technical Intelligence
Washington, D.C.   20301

Defense Nuclear Agency/SPSS
ATTN: Dr. Michael Shore
6801 Telegraph Road
Alexandria, VA   22310

AFTAC/CA (STINFO)
Patrick AFB, FL 32925-6001

TACTEC
Battelle Memorial Institute
505 King Avenue
Columbus, OH 43201   (Final report only)

Mr. Alfred Lieberman
ACDA/VI-OA State Department Building
Room 5726
320 - 21St Street, NW
Washington, D.C.   20451